A Novel Extended Covalent Tripod for Assembling Nine-Coordinate Lanthanide(III) Podates: A Delicate Balance between Flexibility and Rigidity

Sylvain Koeller,[a] Gérald Bernardinelli,[b] Bernard Bocquet,[a] and Claude Piguet*[a]

Abstract: The introduction of long semirigid spacers between the capping carbon atom of the tripod and the unsymmetrical tridentate binding units provides the novel, extended covalent podand tris-{2-[2-(6-diethylcarbamoylpyridin-2-yl)-1-ethyl-1H-benzoimidazol-5-yl-methoxy]ethyl}methane (L^{15}). Reaction of L^{15} with lanthanide(III) in acetonitrile produces stable podates $[Ln(L^{15})]^{3+}$ (Ln = La–Lu) in which three tridentate binding units are facially organized. These wrap around the nine-coordinate pseudo-tricapped trigonal-prismatic metal ions. The crystal structure of $[La(L^{15})](ClO_4)_3$ (**18**, $LaC_{67}H_{82}N_{12}O_{18}Cl_3$, trigonal, $R3c$, $Z = 6$) reveals the formation of a C_3-symmetrical triple-helical podate. Two slightly different arrangements of the flexible ethylenoxy parts of the spacer are observed in the solid state in agreement with the formation of two conformational isomers (**M**:**m**) in a 4:1 ratio. A qualitative analysis of the aromatic diamagnetic anisotropies affecting the NMR signals of $[Ln(L^{15})]^{3+}$ (Ln = La, Y, Lu) in solution, combined with the quantitative determination of electron-induced relaxation in the paramagnetic complex $[Nd(L^{15})]^{3+}$, demonstrate that the solid state structure is maintained in solution. This leads to a mixture of two triple-helical conformers of similar stabilities and that do not interconvert on the NMR timescale between 243 and 343 K. Particular attention has been given to the structural programming of extended covalent tripods for facially organizing unsymmetrical tridentate binding units around Ln^{III}. Photophysical measurements show that L^{15} efficiently protects the metallic coordination spheres and sensitizes Eu^{III} and Tb^{III} upon UV irradiation.

Keywords: chelates · helical structures · lanthanides · N ligands

Introduction

Since the valence 4f orbitals of the lanthanide metal ions (Ln^{III}, electronic configurations $[Xe]4f^n$) are shielded from external perturbations by the outer filled $5s^2$ and $5p^6$ shells,[1] the Ln–ligand dative bonds are mainly electrostatic with only minor covalent contributions resulting from the minute mixing of 4f and ligand-centered wavefunctions.[2] The electronic, spectroscopic, and magnetic properties of the free trivalent ions are thus essentially maintained in their complexes, and lead to functional devices with predetermined properties.[3] Interestingly, the number, nature, and arrangement of the donor atoms in the first coordination sphere produce weak crystal-field effects ($10–400\ cm^{-1}$),[4] which allow an ultrafine tuning of the electronic properties as demonstrated by the recent rational design of energy transfer processes,[5] emission quantum yields,[6] and magnetic anisotropies[7] in lanthanide complexes. However, the ultimate programming of crystal-field parameters relies on a precise structural control of the metallic site, which is difficult to achieve owing to the poor stereochemical preferences of Ln^{III}, and to their tendency to adopt large and variable coordination numbers.[2, 3, 8] In this context, the semirigid tridentate aromatic chelating units $L^1–L^5$ have attracted considerable interest during the last decade. Wrapping of the strands in the D_3-symmetrical complexes $[Ln(L^1\text{-}2H)_3]^{3-}$ and $[Ln(L^i)_3]^{3+}$ ($i = 2–5$) provides stable and well-defined nine-coordinate tricapped trigonal prismatic lanthanide sites.[9] However, the expected formation of a 1:3 statistical mixture of facial and meridional isomers in $[Ln(L^6)_3]^{3+}$ prevents further molecular and crystal-field programming with unsymmetrical tridentate ligands.[10] A straightforward solution considers the connection of the unsymmetrical binding units to a tripod. Three bidentate chelating units have been indeed facially organized for the preparation of unsaturated C_3-symmetrical hexadentate[11] and heptadentate[12] lanthanide complexes working as contrast agents for magnetic resonance imaging (the vacant

[a] Prof. Dr. C. Piguet, Dr. S. Koeller, B. Bocquet
Department of Inorganic, Analytical and Applied Chemistry
University of Geneva, 30 quai E. Ansermet
1211 Geneva 4 (Switzerland)
Fax: (+41) 22-702-6830
E-mail: claude.piguet@chiam.unige.ch

[b] Dr. G. Bernardinelli
Laboratory of X-ray crystallography
University of Geneva, 24 quai E. Ansermet
1211 Geneva 4 (Switzerland)

Supporting information for this article is available on the WWW under http://www.chemeurj.org/ or from the author. Table S1 lists the ES-MS peaks observed during titrations, Table S2 lists elemental analyses for complexes **11**–**17**, and Table S3 collects structural data for the lanthanum coordination sphere in $[La(L^{15})](ClO_4)_3$ (**18**). Figure S1 displays a view of the unit cell in **18** and Figure S2 shows a stereoview of the major isomer of **18** with thermal ellipsoids.

0947-6539/03/0905-1062 $ 20.00+.50/0

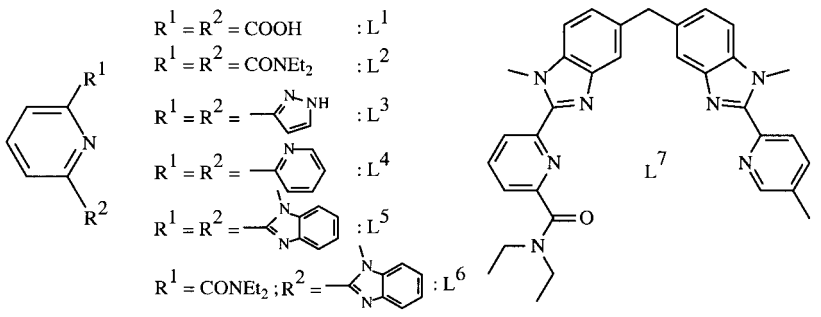

positions being occupied by exchangeable solvent molecules). The application of this concept to tridentate binding units is more difficult, because the helical wrapping of the strands resulting from their complexation to nine-coordinate Ln^{III} induces specific steric constraints within the tripod. This prevents efficient complexation. Adaptable triple-helical pseudo-octahedral $[M^{II}(\alpha,\alpha'\text{-diimine})]$ moieties have been designed as noncovalent tripods for facially organizing three unsymmetrical tridentate binding units analogous to L^6 around nine-coordinate Ln^{III} in the self-assembled triple-stranded helicates $[LnM(L^7)_3]^{5+}$ (M^{II} = Fe, Co, Zn).[13] However, these systems exist as dynamic libraries in solution, and their extreme sensitivity to external conditions limits their use as functional devices.[14] The replacement of the noncovalent tripod with a covalent tris(2-aminoethyl)amine tripod (TREN) has been first explored for L^8[15] and L^9;[16] these give the podates $[Ln(L^i\text{-}3H)]$ in the solid state. The introduction of a central pyridine ring in L^{10}[17] and L^{11}[18] provides fused five-membered chelate rings that stabilize the final podates $[Ln(L^i)]^{3+}$. Attempts to favor helical wrapping with a longer tripod in L^{12} failed, thus leading to flexible podates in solution.[19] Recently, two water-stable nine-coordinate lanthanide podates $[Ln(L^{13}\text{-}3H)]$[20] and $[Ln(L^{14}\text{-}3H)]$[21] were reported; these compounds take advantage of rigid macrocyclic triazacyclononane platforms grafted with carboxylate-containing side arms. However, the design of a helical tripod possessing a single capping atom for organizing three unsymmetrical tridentate binding units around Ln^{III} remains a challenge for the preparation of directional polymetallic d–f[22] and f–f[23] light-converting devices. In this paper, we consider an alternative strategy in which the spacers contain a sequence of aromatic and aliphatic carbon atoms controlling the balance between rigidity and flexibility in the tripod. Particular attention is focused on the consequences of the mechanical coupling occurring between the covalent tripod and the tridentate binding units for programming the helical wrapping of the strands in the podates $[Ln(L^{15})]^{3+}$.

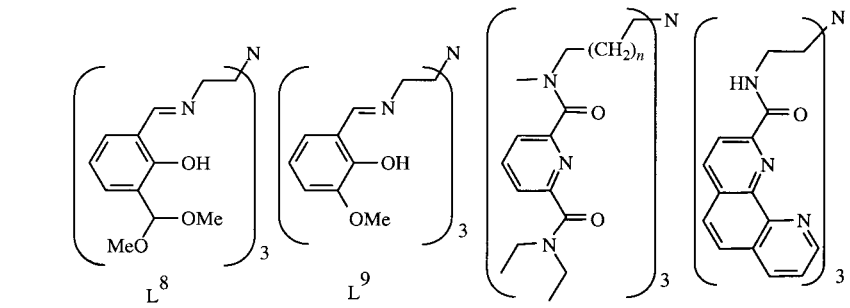

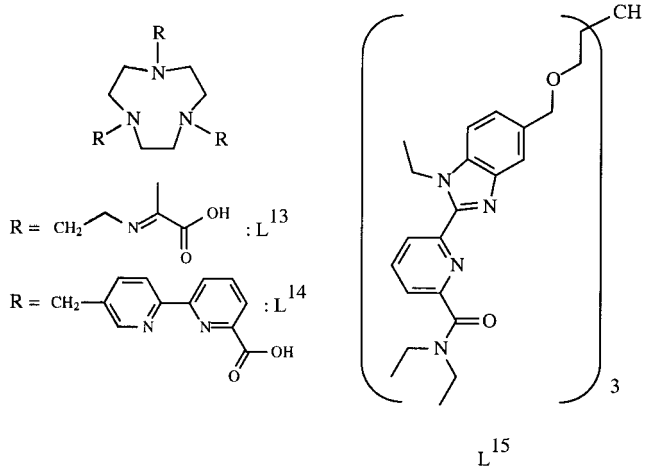

Results and Discussion

Synthesis of the ligand $L^{15}\cdot H_2O$: A methine group has been introduced as the capping atom in the tripod and ether connectors ensure the fixation of the side arms. Firstly, this prevents the complications associated with the protonation of the capping nitrogen atom previously encountered with $[Ln(L^{10}+H)]^{4+}$,[17] and secondly it limits de-activation of metal-centered excited states by high-energy NH vibrations in the final complexes.[24] The podand tris-{2-[2-(6-diethylcarbamoylpyridin-2-yl)-1-ethyl-1H-benzoimidazol-5-yl-methoxy]ethyl}methane monohydrate ($L^{15}\cdot H_2O$) is obtained in fourteen steps according to a convergent strategy in which three unsymmetrical side arms **7** are connected to the covalent tripod **10** during the last step, as shown in Scheme 1. The tridentate unit **7** is prepared from the unsymmetrical synthon **3**[25] and *o*-nitro-*N*-ethylaminoarene **2**[26] according to a modified Philips reaction.[27] The tripod **10** is obtained is three steps from the commercially available compounds **8** and **9**.[28] All methylene protons in L^{15} are enantiotopic on the NMR timescale, thus pointing to a flexible behavior in solution compatible with an average C_{3v} symmetry.

Formation and isolation of the complexes $[Ln(L^{15})](ClO_4)_3\cdot nH_2O$ (Ln = La, *n* = 1: 11; Ln = Nd, *n* = 1: 12; Ln = Eu, *n* = 1: 13; Ln = Gd, *n* = 1: 14; Ln = Tb, *n* = 1: 15; Ln = Lu, *n* = 4: 16;

  0947-6539/03/0905-1063 $ 20.00+.50/0

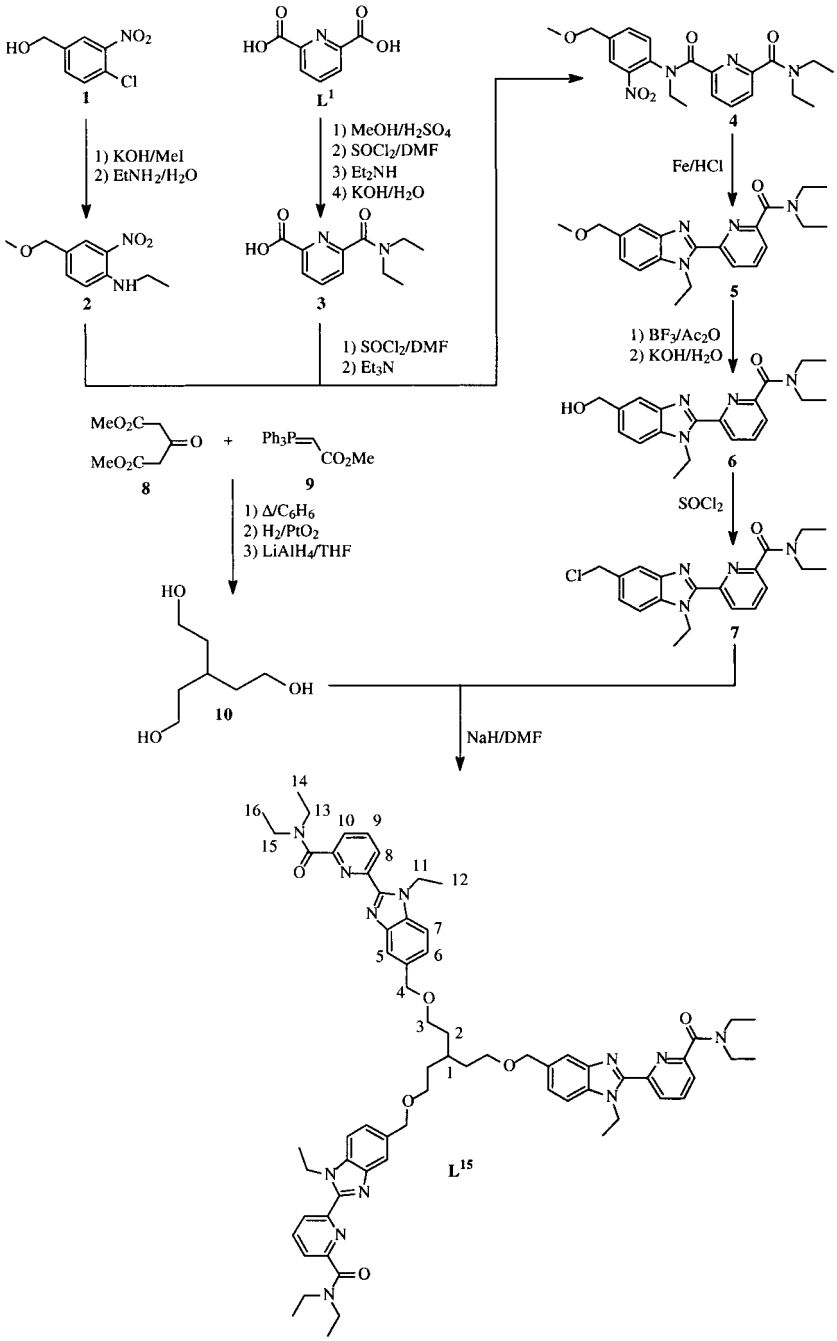

Scheme 1. Multi-step synthesis of L^{15} with numbering scheme for NMR measurements.

Ln = Y, n = 1: 17): ESI-MS titrations of $L^{15}\cdot H_2O$ (10^{-4} mol dm^{-3}, acetonitrile) with $Ln(CF_3SO_3)_3\cdot xH_2O$ (Ln = La, Eu, Lu; $x = 1-4$) for Ln:L^{15} ratios in the range 0.5–2.0 show the exclusive formation of the complex $[Ln(L^{15})]^{3+}$ together with its adduct ions $[Ln(L^{15})(CF_3SO_3)_n]^{(3-n)+}$ (n = 1–2). The replacement of triflate counterions with poorly coordinating perchlorate anions has no significant effect on the complexation process, and the ESI-MS spectra display the peaks corresponding to $[Ln(L^{15})(ClO_4)_n]^{(3-n)+}$ ($n = 0-2$) (See Table S1, Supporting Information). Spectrophotometric titrations of $L^{15}\cdot H_2O$ (10^{-4} mol dm^{-3} in acetonitrile and 0.01 mol dm^{-3} $[N(nBu)_4]ClO_4$) with $Ln(ClO_4)_3\cdot xH_2O$ (Ln = La, Pr, Nd, Sm, Gd, Dy, Er, Lu; $x = 6-8$) show a smooth evolution of the absorption spectra for Ln:L^{15} in the range 0.1–1.0 with a single sharp end point for Ln:L^{15} = 1.0 (Figure 1b). The observation of three isosbestic points at 245, 274, and 327 nm (Figure 1a) indicates the existence of the free ligand together with a single absorbing complex in solution; this complex can be safely assigned to $[Ln(L^{15})]^{3+}$ in agreement with ESI-MS results. The spectrophotometric data can be fitted with non-linear least-squares techniques to the equilibrium shown in Equation (1).[29]

$$Ln^{3+} + L^{15} \rightleftharpoons [Ln(L^{15})]^{3+} \qquad \log(\beta_{11}^{Ln}) \qquad (1)$$

The formation constants $\log(\beta_{11}^{Ln}) = 6.5-7.6$ do not vary significantly along the lanthanide series within experimental errors and point to negligible size-discriminating effects (Table 1). They can be compared with $\log(\beta_{11}^{Ln}) = 6.5-6.6$ obtained in pure acetonitrile for $[Ln(L^{11})]^{3+}$ (Ln = Ce–Eu),[18] in which Ln^{III} is also in a nine-coordinate environment surrounded by six heterocyclic nitrogen atoms and three oxygen atoms of carboxamide groups, and with

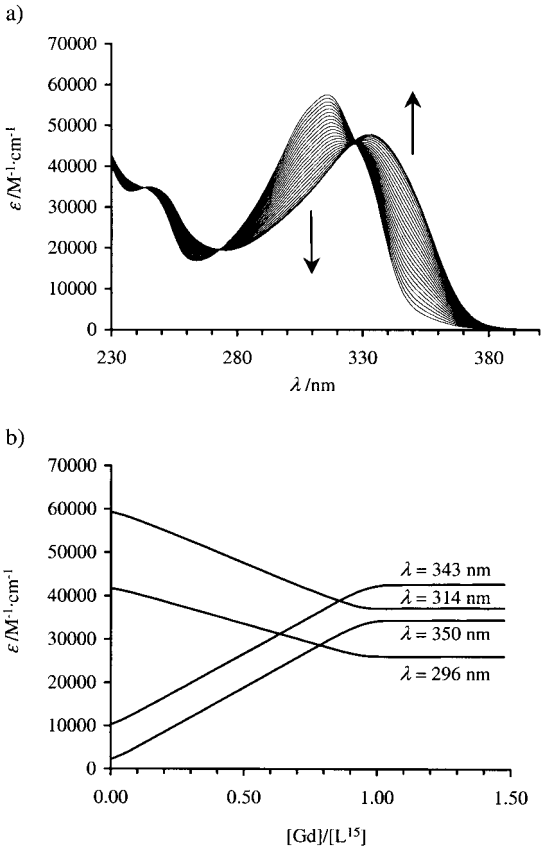

Figure 1. a) Variation of absorption spectra observed for the spectrophotometric titration of $L^{15}\cdot H_2O$ (10^{-4} mol dm^{-3} in acetonitrile + 0.01 mol dm^{-3} $[N(nBu)_4]ClO_4$) with $Gd(ClO_4)_3\cdot 6.6H_2O$ at 298 K (Gd:L^{15} = 0.1–1.5). b) Corresponding variation of observed molar extinctions at four different wavelengths.

0947-6539/03/0905-1064 $ 20.00+.50/0 *Chem. Eur. J.* **2003**, *9*, No. 5

Table 1. Formation constants $\log(\beta_{11}^{Ln})$ for the complexes $[Ln(L^{15})]^{3+}$ in acetonitrile (0.01 mol dm^{-3} $[N(n\mathrm{Bu})_4]ClO_4$, 293 K).

Ln^{III}	$\log(\beta_{11})$	Ln^{III}	$\log(\beta_{11})$
La^{III}	7.0 ± 0.2	Gd^{III}	7.6 ± 0.3
Pr^{III}	7.3 ± 0.4	Dy^{III}	7.2 ± 0.2
Nd^{III}	6.5 ± 0.3	Er^{III}	7.5 ± 0.4
Sm^{III}	6.8 ± 0.3	Lu^{III}	6.8 ± 0.3

$\log(\beta_{11}^{Ln}) = 6.7-8.5$[17] and $\log(\beta_{11}^{Ln}) = 6.4-7.1$[19] obtained for $[Ln(L^{10})]^{3+}$ and $[Ln(L^{12})]^{3+}$ (Ln = La – Lu), respectively. In this case, six oxygen atoms and three heterocyclic nitrogen atoms are complexed to Ln^{III}. Although strict comparisons are limited by the different ionic strengths used for recording the spectroscopic data, the similar formation constants found for these podates indicate that the length of the spacer (*l*) within the tripod has only minor effects on the stability of the final complexes (*l* is defined as the number of atoms separating the apical atom and the first coordinated atom, for example $l = 4$ for $[Ln(L^{10})]^{3+}$ and $[Ln(L^{11})]^{3+}$, $l = 5$ for $[Ln(L^{12})]^{3+}$ and $l = 7$ for $[Ln(L^{15})]^{3+}$). Moreover, the rigid aromatic phenyl rings incorporated in the tripod of $[Ln(L^{15})]^{3+}$ do not induce dramatic steric constraints precluding an efficient wrapping of the strands around Ln^{III}.

Diffusion of diethyl ether into concentrated solutions of the complexes in acetonitrile provides microcrystalline powders of $[Ln(L^{15})](ClO_4)_3 \cdot nH_2O$ (Ln = La, $n = 1$: **11**; Ln = Nd, $n = 1$: **12**; Ln = Eu, $n = 1$: **13**; Ln = Gd, $n = 1$: **14**; Ln = Tb, $n = 1$: **15**; Ln = Lu, $n = 4$: **16**; Ln = Y, $n = 1$: **17**) in 72–93% yield. Elemental analyses support the proposed formulations (see Table S2, Supporting Information). IR spectra display the vibrations typical of the coordinated tridentate benzimidazole–pyridine–carboxamide binding unit (ν(C=O) = 1585–1590 cm^{-1}, ν(C=N) = 1570–1574 cm^{-1})[13] together with bands at 1090 and 625 cm^{-1} typical of ionic perchlorates.[30] Fragile anhydrous monocrystals suitable for X-ray diffraction studies were obtained for $[Ln(L^{15})](ClO_4)_3$ (Ln = La, **18**; Ln = Eu, **19**) upon ultra-slow diffusion of diethyl ether into concentrated acetonitrile solutions under a dry atmosphere.

Crystal and molecular structure of $[Ln(L^{15})](ClO_4)_3$ (Ln = La, 18; Ln = Eu, 19): The complexes $[Ln(L^{15})](ClO_4)_3$ (Ln = La, **18**; Ln = Eu, **19**) are isostructural, but the monocrystals obtained for Ln = La (**18**) were of higher quality and the X-ray diffraction study has been focused on this complex. The crystal structure of **18** confirms the formation of the cationic 1:1 complex $[La(L^{15})]^{3+}$ together with disordered ionic perchlorate anions (see Experimental Section). The $[La(L^{15})]^{3+}$ cation is located on a crystallographic threefold axis passing through C1 and La (special positions 6a). Figure 2 shows views of the cations perpendicular to the threefold axis and Table 2 collects together selected bond lengths and bond angles.

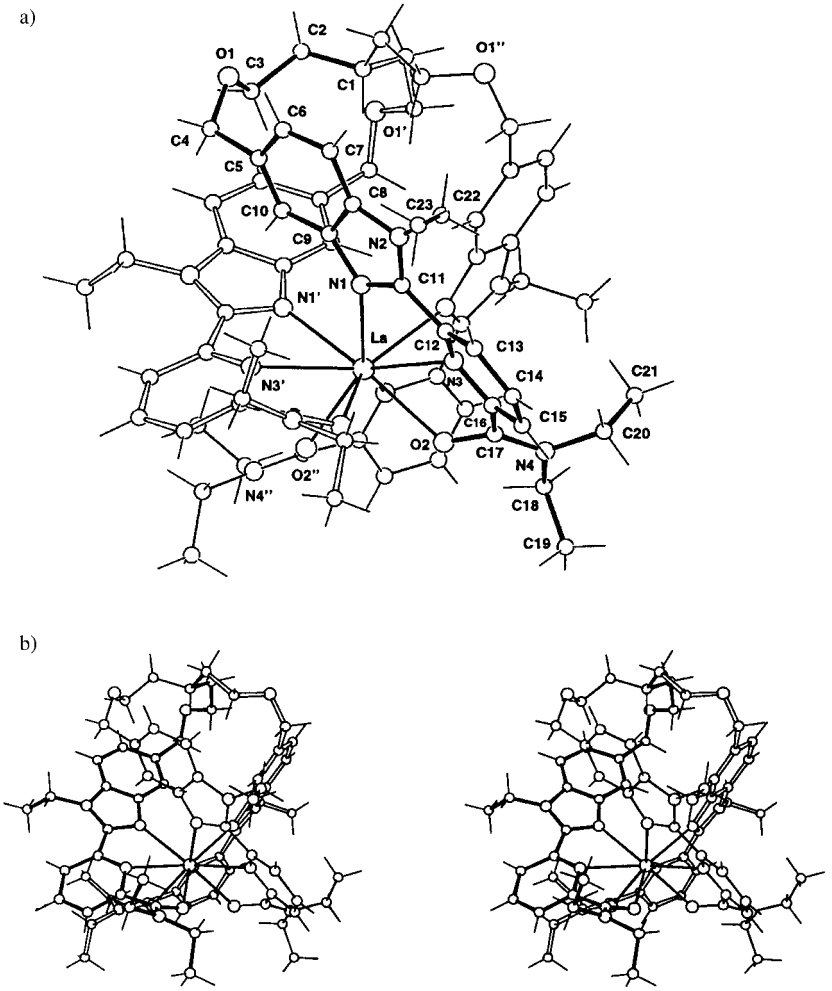

Figure 2. a) Perspective view of the $[La(L^{15})]^{3+}$ ion perpendicular to the threefold axis showing the atomic numbering scheme (the indexes ′ and ″ denote the symmetry related strands). b) Stereoview of the major conformer (**M**) perpendicular to the threefold axis.

Table 2. Selected bond lengths [Å] and bond angles [°] in $[La(L^{15})](ClO_4)_3$ (**18**).[a]

La–N1	2.665(6)	O2-La-N3″	70.2(3)
La–N3	2.695(8)	O2-La-N1′	145.0(3)
La–O2	2.486(7)	O2-La-N1″	79.5(3)
N1-La-N3	61.3(2)	N1-La-N1′	87.3(2)
N3-La-O2	62.5(2)	N1-La-N3′	75.0(2)
N1-La-O2	123.8(2)	N1-La-N3″	144.1(2)
O2-La-O2′	81.3(3)	N3-La-N3′	119.9(2)
O2-La-N3′	136.3(2)	La···C1[b]	7.03(4)

[a] The indexes ′ and ″ denote the symmetry related strands (see Figure 2). [b] Nonbonded distance.

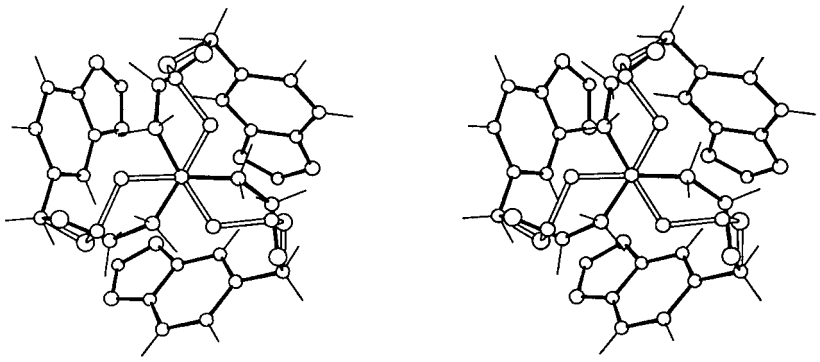

Figure 3. Partial stereoview of the complex $[La(L^{15})]^{3+}$ along the threefold axis showing the two conformers **M** (full line) and **m** (empty line).

The C2, C3, and O1 atoms display a significant disorder, which can be solved with the refinement of two distinct atomic sites for each atom (occupancy factors 0.8/0.2, see Experimental Section) corresponding to two different conformations of the tripod. These will be refered to as a major (**M**, 80%) and a minor (**m**, 20%) conformer (see Figure 3). No significant residual peak in the Fourier difference analysis is located close to C1, and the displacement parameters of C1 are almost isotropic (the r.m.s.d. for C1 parallel and perpendicular to the C_3 axis amount to 0.33 and 0.37 Å, respectively). We can therefore exclude an *exo* arrangement of the C1–H bond and both conformers adopt the *endo* conformation of the apical methine group with its hydrogen atom pointing toward La^{III}, as previously reported for the protonated capping nitrogen atom in $[Eu(L^{10}+H)]^{4+}$.[17]

A careful examination of Figure 3 reveals that the two conformers display different wrapping of the ethyleneoxy spacers connecting the apical methine group and the rigid aromatic benzimidazole side arms. The helical threads in the major conformer **M** adopt a single screw direction (except within the small O1–C4 portion in which no significant helical twist occurs), thus leading to an overall regular triple-helical arrangement of the tripod. Conversely, the ligand threads of the minor conformer **m** invert their screw direction between the C2–C3 and C3–O1 portions and provide two successive domains with opposite helicities within the tripod (an amphiverse triple-helical arrangement).[31] A detailed quantitative structural analysis of the helical revolution of the threads about the threefold axis in $[La(L^{15})]^{3+}$ requires the use of seven parallel facial planes F1–F7 defined by the symmetry related atoms of the three strands. The coordination sphere around La^{III} is sliced into two helical portions delimited by the three facial planes F1 {O2,O2′,O2″}, F2 {N3,N3′,N3″}, and F3 {N1,N1′,N1″}, while the covalent tripod is further delimited by F4 {C4,C4′,C4″}, F5 {O1,O1′,O1″}, F6 {C3,C3′,C3″}, and F7 {C2,C2′,C2″}. The interplanar distance d_{ij} corresponds to the linear progression of the strand along the helical axis within each part limited by F_i and F_j. The ω_{ij} angles between the projections of the X_i and Y_j atoms of the same strand belonging to the different planes F_i and F_j measure the angular rotation.[17] The pitch of each helical portion can be then calculated according to $P_{ij}=(d_{ij}/\omega_{ij})\times 360$ (see Table 3). P_{ij} corresponds to the length of a cylinder containing a single turn of the helix defined by the geometrical characteristics d_{ij} and ω_{ij}. The helical twist of the tridentate binding units defined by F1–F2 and F2–F3 is regular, but the associated pitches $P_{12}=10.11$ Å and $P_{23}=12.14$ Å are slightly shorter than those reported for $[Eu(L^{10}+H)]^{4+}$ (11.84 Å and 13.30 Å).[17] This points to a tighter wrapping process in $[La(L^{15})]^{3+}$ induced by the longer tripod. In the rigid aromatic F3–F4 portion, the helical twist is significantly reduced ($P_{34}=22.1$ Å) and it even stops in the next F4–F5 domain for the major **M** conformer before its restoration in the final portions F5–F6 and F6–F7 of the tripod. For the minor **m** conformer, a tight helical twist is maintained in the F4–F5 portion, but inversion of the screw sense occurs within the F5–F6 domain and opposite helicity characterizes the terminal F6–F7 portion (as shown in Figure 3). A rough CPK molecular modeling of the podate $[La(L^{15})]^{3+}$ suggests that the interconversion of the two isomers requires a considerable distortion of bond lengths and bond angles within the tripod.

Table 3. Helical pitches P_{ij}, linear distances d_{ij}, and average twist angle ω_{ij} along the C_3 axis for the major (**M**) and minor (**m**) conformers in the crystal structure of $[La(L^{15})]^{3+}$.[a]

Helical portion[b]	Conformer	d_{ij} [Å]	ω_{ij} [°]	P_{ij} [Å]
F1–F2	**M** = **m**	1.53	54.6	10.11
F2–F3	**M** = **m**	1.71	50.8	12.14
F3–F4	**M** = **m**	3.72	60.6	22.10
F4–F5	**M (m)**	1.27 (0.46)	2.8 (19.0)	162.51 (8.64)
F5–F6	**M (m)**	0.11 (1.38)	23.1 (2.4)	1.75 (206.47)
F6–F7	**M (m)**	1.00 (0.01)	15.2 (31.9)	23.69 (0.14)

[a] Each helical portion F*i*–F*j* is characterised by i) a linear extension d_{ij} defined by the separation between the facial planes, ii) an average twist angle ω_{ij} defined by the angular rotation between the projections of N*i* and N*j* (or O*j*) belonging to the same ligand strand, and iii) its pitch P_{ij} defined as the ratio of axial over angular progressions along the helical axis (see text). [b] F1:{O2, O2′, O2″}; F2:{N3, N3′, N3″}; F3:{N1, N1′, N1″}; F4:{C4, C4′, C4″}; F5:{O1, O1′, O1″}; F6:{C3, C3′, C3″}; F7:{C2, C2′, C2″}.

In the solid state, the two conformers display the same metallic environment in which the La atom is nine-coordinate in a distorted tricapped trigonal prismatic site with the three oxygen atoms of the carboxamide groups and the three nitrogen atoms of the benzimidazole rings occupying the vertices of the prism, and the three nitrogen atoms of the pyridine rings capping the rectangular faces. The La–N(py), La–N(bzim), and La–O(amide) bond lengths are standard and closely match those found in the related noncovalent podate $[LaCo(L^{7})_3]^{6+}$ in which the tripod is constituted by an inert triple-helical pseudooctahedral $[Co^{III}(\alpha,\alpha'?diimine)_3]$ moiety (Figures 4a and b).[32] The detailed structural analysis of the tricapped trigonal prismatic lanthanide site based on the classical determination of the ϕ, θ_i, and ω_i angles[9a, 13, 33] shows only faint differences between $[LaCo(L^{7})_3]^{6+}$ and $[La(L^{15})]^{3+}$. This is in agreement with comparable helical wrappings of the tridentate binding units (see Table S3,

0947-6539/03/0905-1066 $ 20.00+.50/0 *Chem. Eur. J.* **2003**, *9*, No. 5

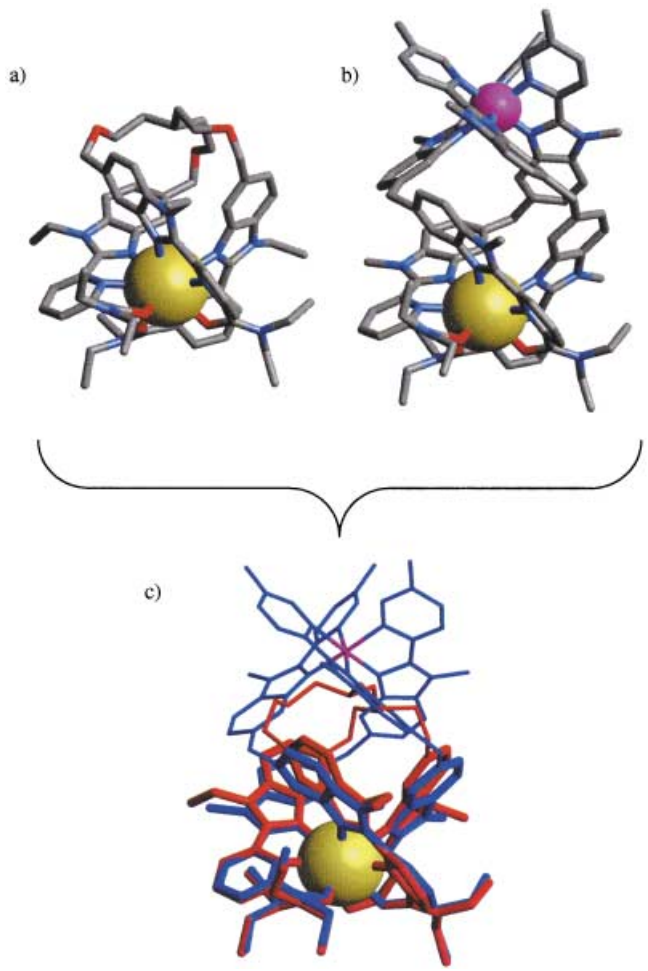

Figure 4. Perspective views of the crystal structures of a) $[La(L^{15})]^{3+}$ (**M** conformer), and b) $[LaCo(L^{7})_3]^{6+}$[32] perpendicular to the C_3 axis. c) Optimized superposition of the two binding domains of $[LaCo(L^{7})_3]^{6+}$ (in blue) and $[La(L^{15})]^{3+}$ (in red) highlighting the minor contraction of the upper triangular face of the trigonal prism in $[La(L^{15})]^{3+}$.

Supporting Information). The main discrepancy concerns a slightly tighter arrangement of the benzimidazole rings induced by the shorter covalent tripod in $[La(L^{15})]^{3+}$. This forces the six-membered phenyl rings to come closer to the threefold axis as exemplified in Figure 4c. As a result of the helical wrapping of the strands, the pyridine ring of each strand is not coplanar with the adjacent benzimidazole ring (interplanar angle: 25°) and carboxamide group (interplanar angle: 45°). This helical twist prevents an adequate alignment of the lone pair of the pyridine nitrogen atom with the La–N(py) bond (La^{III} lies 1.33 Å outside the plane of the pyridine ring) as similarly observed for $[LaCo(L^{7})_3]^{6+}$.[32] However, the La atom almost lies in the intermediate F2 plane defined by the three pyridine nitrogen atoms (deviation 0.105(3) Å toward F3) in $[La(L^{15})]^{3+}$ as is observed similarly for La^{III} in $[LaCo(L^{7})_3]^{6+}$ (0.104 Å toward F3).[32] We conclude that the length of the spacers in the covalent tripod of L^{15} ($l = 7$ atoms) is compatible with the regular wrapping of the three strands around the nine-coordinate La^{III} as observed in the self-assembled helicate $[LaCo(L^{7})_3]^{6+}$, which possesses even longer spacers ($l = 8$). This contrasts with the considerable sterical constraints induced by the short TREN tripod ($l = 4$) and the resulting conical triple-helical arrangement of the strands found in $[Eu(L^{10}+H)]^{4+}$.[17] However, the two different conformations observed in the solid state for the ethyleneoxy groups in the two conformers of $[La(L^{15})]^{3+}$ suggest some residual strains within the tripod. In the unit cell, $[La(L^{15})]^{3+}$ ions with opposite helicities are alternatively packed into columns running along the *c* direction (see Figure S1, Supporting Information).

Solution structure of the complexes $[Ln(L^{15})](ClO_4)_3 \cdot nH_2O$ (Ln = La, *n* = 1: 11; Ln = Nd, *n* = 1: 12; Ln = Eu, *n* = 1: 13; Ln = Lu, *n* = 4: 16; Ln = Y, *n* = 1: 17): We have previously shown by ESI-MS and spectrophotometry that the complexation of L^{15} to the diamagnetic Ln^{III} (Ln = La, Lu, Y) gives exclusively $[Ln(L^{15})]^{3+}$ in acetonitrile, but their ^{1}H NMR spectra systematically display two different sets of sixteen signals corresponding to two different C_3-symmetrical species in approximately 70:30% ratios (see Table 4). The ^{13}C NMR spectra confirm the existence of two C_3-symmetrical species, each displaying 23 signals. The minor variation of the chemical shifts of the same nucleus in the two isomers points to similar chemical environments and closely related arrangements of the strands (as shown in Table 4 and Figure 5). From

Table 4. ^{1}H NMR shifts (with respect to $SiMe_4$) of L^{15} and its complexes $[Ln(L^{15})](ClO_4)_3 \cdot nH_2O$ (Ln = La, *n* = 1: **11**; Ln = Nd, *n* = 1: **12**; Ln = Eu, *n* = 1: **13**; Ln = Lu, *n* = 4: **16**; Ln = Y, *n* = 1: **17**) in CD_3CN at 298 K.[a]

	%[b]	H1	H2	H3	H4	H5	H6	H7	H8	H9	H10	H11	H12	H13	H14	H15	H16
L^{15}	100	1.79	1.57	3.51	4.51	7.62	7.25	7.42	7.46	7.95	8.30	4.69	1.33	3.51	1.20	3.28	0.99
11	71 (**M**)	0.02	0.74	2.45	3.62, 4.13	6.28	7.35	7.74	7.93	8.40	8.29	4.77	1.70	3.49	1.06	2.88	0.80
11	29 (**m**)	0.48	0.74	2.70	3.20, 4.37	6.02	7.43	7.81	7.95	8.42	8.34	4.77	1.70	3.49	1.06	2.88	0.80
12	66 (**M**)	−0.63	−0.09	1.87	2.88, 3.58	2.11	6.90	8.27	8.97	9.49	10.50	3.06 3.35	−0.09 4.23	3.91	1.49	5.22	2.18
12	34 (**m**)	−2.09	−0.09	1.87	2.34, 3.81	2.11	6.93	8.33	9.04	9.62	10.71	3.06 3.35	−0.09	3.91 4.23	1.49	5.22	2.18
13	67 (**M**)	1.70	1.63	3.82	4.59, 4.78	10.04	6.60	7.91	4.79	6.79	6.04	4.19 4.33	1.10	2.62 3.04	0.47	2.48 2.78	2.03
13	33 (**m**)	3.05	1.63	3.82	4.40, 5.08	10.04	6.67	8.00	4.66	6.72	6.00	4.19 4.33	1.10	2.62 3.04	0.47	2.48 2.78	2.03
16	68 (**M**)	0.40	0.60	2.37	3.70, 4.08	5.75	7.31	7.73	7.98	8.40	8.40	4.83	1.74	3.55	1.11	2.68	0.76
16	32 (**m**)	−0.29	0.60	2.54	3.37, 4.34	5.60	7.38	7.80	7.98	8.40	8.40	4.83	1.74	3.55	1.11	2.68	0.76
17	64 (**M**)	0.43	0.61	2.71	3.66, 4.08	5.81	7.31	7.72	7.94	8.36	8.36	4.81	1.73	3.52	1.08	2.75	0.76
17	36 (**m**)	−0.28	0.61	2.71	3.32, 4.34	5.67	7.38	7.79	7.94	8.36	8.36	4.81	1.73	3.52	1.08	2.75	0.76

[a] See Scheme 1 for the numbering scheme. [b] Ratio of the two isomers according to the integration of ^{1}H NMR signals (error ±3%).

  0947-6539/03/0905-1067 $ 20.00+.50/0

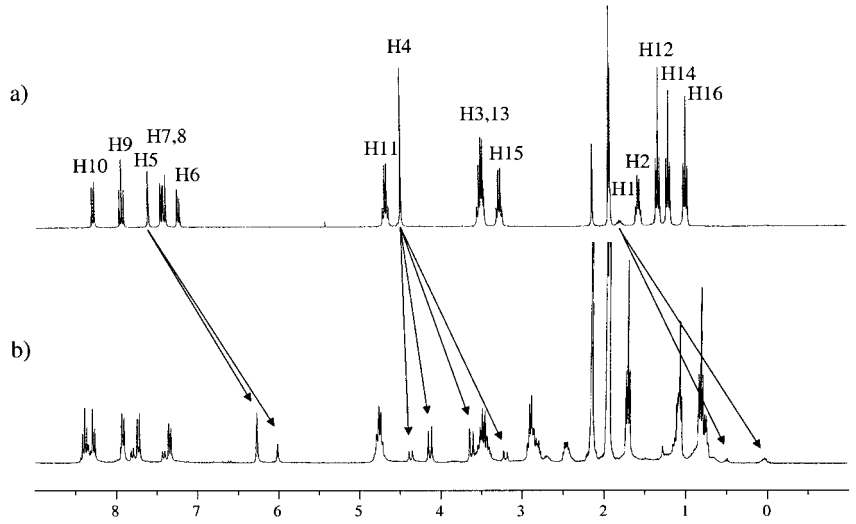

Figure 5. ^{1}H NMR spectra of a) L^{15} and b) $[La(L^{15})]^{3+}$ in CD_3CN (298 K).

the average 7:3 equilibrium distribution observed between the two isomers in $[Ln(L^{15})]^{3+}$ (Ln = La, Lu, Y, Table 4), a difference in free energy of $\Delta G = 2.1$ kJ mol^{-1} can be calculated. Surprisingly, variable temperature NMR spectroscopy (243–343 K) does not show significant variations of the spectra in agreement with a considerable free energy of activation ($\Delta G^{\neq}$) for the interconversion process. Taking into account the difference in chemical shift between the NMR signals of H5 (singlets) in the two isomers of $[La(L^{15})]^{3+}$ ($\delta\nu$(La) = 78 Hz, Table 4) and the difference in population between the two exchangeable sites $\Delta p = 0.4$, the polynomial expression of Equation (2) gives $X = 2.18$. The classical Equations (3) and (4) allow an estimation of the maximum value for the rate constant $k \ll 112$ s^{-1} associated with a minimum free energy of activation $\Delta G^{\neq}$(La) $\gg$ 71 kJ mol^{-1} for the interconversion process at the highest accessible temperature in acetonitrile ($T = 343$ K and k_B and h are respectively the Boltzmann and the Planck constants).[34]

$$X^6 - 6X^4 + [12 - 27(\Delta p)^2]X^2 - 8 = 0 \quad (2)$$

$$k = \frac{\pi\delta\nu}{X} \quad (3)$$

$$\Delta G^{\neq} = RT\ln\left(\frac{k_B T}{kh}\right) \quad (4)$$

These results suggest that the two isomers observed in solution for $[Ln(L^{15})]^{3+}$ (Ln = La, Y, Lu) display comparable ground-state energies, but that low-energy dynamic processes are not accessible for their interconversion on the NMR timescale.

Further structural information can be gained from the detailed analysis of the complexation shifts and the diastereotopic probes in the diamagnetic complexes $[Ln(L^{15})]^{3+}$ (Ln = La, Lu, Y). Compared to the ^{1}H NMR spectrum of the free ligand L^{15}, the complexation of Ln^{III} (Ln = La, Lu, Y) induces four remarkable changes.

1) The complexation process provides two noninterconverting isomers (on the NMR timescale) in a 7:3 ratio as previously discussed.
2) The enantiotopic methylene protons of the free ligands (H2, H3, H4, H11, H13 and H15) become diastereotopic in the two isomeric forms of the complexes $[Ln(L^{15})]^{3+}$, leading to i) interpenetrated ABX_3 spin systems for the ethyl residues (H11-H12, H13-H14 and H15-H16); ii) intractable ABCDX spin systems for the protons of the tripods (H1-H2-H3) and iii) much simpler AB spin systems for the isolated methylene H4 (Figure 5). These observations show that the three strands wrap around Ln^{III} to give C_3-symmetrical $[Ln(L^{15})]^{3+}$ complexes that do not exhibit fast $P \rightleftharpoons M$ intramolecular helical interconversion on the NMR timescale at 298 K. Variable temperature spectra (233–343 K) do not affect the signals of the diastereotopic protons and a calculation using Equations (2–4) for this dynamic process with $\delta\nu$(H4) = 153 Hz (Table 4), $\Delta p = 0$ ($X = \sqrt{2}$)[34] and $T =$ 343 K gives a maximum rate constant $k \ll 340$ s^{-1} associated with a minimum free energy of activation $\Delta G^{\neq}$(La) $\gg$ 68 kJ mol^{-1}. This strongly contrasts with the fast helical interconversion occurring in the triple-helical complex $[La(L^2)_3]^{3+}$ at room temperature($\Delta G^{\neq} < 55$ kJ mol^{-1})[9a] and the coalescence of the methylene protons observed at 323 K for the podate $[La(L^{10})]^{3+}$ ($\Delta G^{\neq}_{323\,K} =$ 66 kJ mol^{-1}).[35] However, no helical interconversion can be detected for the rigid noncovalent podates $[LnCo(L^7)_3]^{6+}$ on the NMR timescale[13c] as found for $[Ln(L^{15})]^{3+}$. This strongly suggests that the covalent tripod in the last complexes is rigid enough to prevent fast helical interconversion, but flexible enough to allow an efficient wrapping of the strands.
3) The isolated aromatic proton H5 is shielded by $\Delta\delta = 1.48$–1.74 ppm (Ln = La), $\Delta\delta = 2.01$–2.16 ppm (Ln = Lu) and $\Delta\delta = 1.95$–2.09 ppm (Ln = Y, Table 4) upon complexation as previously reported for the related proton in $[LnCo(L^7)_3]^{6+}$ ($\Delta\delta = 1.91$ ppm).[13c] This behavior is diagnostic of the wrapping process of the strands which puts H5 in the shielding region of the aromatic imidazole ring of the adjacent strand,[13a] as observed in the crystal structure of $[La(L^{15})]^{3+}$ (Figure 2).
4) The ^{1}H NMR signal of the apical proton H1 is shielded by $\Delta\delta = 1.77$ ppm for the major isomer and $\Delta\delta = 1.31$ ppm for the minor isomer in $[La(L^{15})]^{3+}$ as a result of the conformational change of the tripod occurring upon complexation. In the crystal structure of $[La(L^{15})]^{3+}$ (Figure 2), the capping methine group adopts an *endo* conformation with H1 pointing inside the cavity defined by the three wrapped phenyl rings of the benzimidazole rings. Therefore, H1 lies in the shielding region of the diamagnetic anisotropic tensor associated with aromatic rings, and the observed

0947-6539/03/0905-1068 $ 20.00+.50/0 *Chem. Eur. J.* **2003**, *9*, No. 5

downfield complexation shifts confirm that both isomers adopt related endo conformations in solution. The exact location of H1 slightly changes between the two isomers. It is worth noting that the 7:3 ratio observed for $[La(L^{15})]^{3+}$ in solution is close to the 8:2 ratio observed for the two different conformations of the tripod (**M** and **m**) in the solid-state. We can thus tentatively assign the major isomer observed in solution to the complex displaying a regular triple-helical conformation within its tripod (related to the solid-state **M** conformer). The minor isomer in solution may therefore be assigned to the complex displaying an amphiverse arrangement of the spacers within the tripod (related to the solid-state **m** conformer). Closely related complexation shifts are observed for $[Lu(L^{15})]^{3+}$ and $[Y(L^{15})]^{3+}$ except for minor deviations resulting from the tighter wrapping of the strands around the smaller lanthanide ions as previously reported for $[LnCo(L^{7})_3]^{6+}$.[13c] However, contrary to $[La(L^{15})]^{3+}$, the major isomer for $[Lu(L^{15})]^{3+}$ and $[Y(L^{15})]^{3+}$ in solution corresponds to that with the smaller complexation shift for H1 (Table 4). This strongly suggests that the relative ratio of the two isomers in solution depends on the size of the complexed metal (in other words, the free energy between the ground states of the two conformers varies with the size of Ln^{III}).

A strict analogy between solid-state and solution structures for $[La(L^{15})]^{3+}$ is precluded by the systematic splitting observed for all signals in the NMR spectra of the two isomers. While the solid-state structure implies that only the conformation of the aliphatic part of the tripod significantly changes, the tridentate binding units remaining invariable. However, we suspect that the structure of the podate is relaxed in solution and minor variations in the wrapping of the strands in solution occur because solid-state intermolecular packing forces have been removed. We have thus resorted to electron-induced nuclear relaxation measurements to address reliable Ln–nucleus distances in solution for both isomers.[13a, 36] For fast-relaxing lanthanide complexes (Ln = Ce–Yb, except Gd), the contact relaxation can be neglected and only transcient and static dipolar mechanisms contribute to the induced paramagnetic nuclear relaxation processes.[36, 37] In the fast motion limit and in the absence of chemical exchange processes (two conditions met for $[Ln(L^{15})]^{3+}$),[37] the paramagnetic contribution to the longitudinal relaxation rate of the nucleus i ($1/T_{1i}^{para}$) is given by Equation (5). Here, r_i is the lanthanide–nucleus distance, τ_e and τ_r are the electronic and rotational correlation times, respectively, μ_{eff} is the effective magnetic moment of the complex, and the other terms have their usual meaning.[36, 37] Since both transcient and static dipolar contributions depend on r_i^{-6}, Equation (5) reduces to Equation (6) for a given paramagnetic complex at fixed magnetic field and temperature.[38] For the two conformers of $[Ln(L^{15})]^{3+}$ in acetonitrile, no significant change in τ_e, τ_r, and μ_{eff} is expected. Identical C_j constants can be used, thus leading to Equation (7) for comparing Ln–nucleus distances when T_{1i}^{para} are accessible for the same nucleus in both conformers **M** and **m**. Finally, the paramagnetic contributions to the longitudinal relaxation rates ($1/T_{1i}^{para}$) in the paramagnetic $[Nd(L^{15})]^{3+}$ complex can be extracted from the experimental relaxation rates ($1/T_{1i}^{exp}$) with Equation (8), in which the diamagnetic contributions ($1/T_{1i}^{dia}$) correspond to the relaxation rates of the same nuclei in the analogous diamagnetic complex $[La(L^{15})]^{3+}$ (Table 5).[9a]

$$\frac{1}{T_{1i}^{para}} = \frac{4}{3}\left(\frac{\mu_0}{4\pi}\right)^2 \frac{\gamma_I \mu_{eff}^2 \beta^2}{r_i^6}\tau_e + \frac{6}{5}\left(\frac{\mu_0}{4\pi}\right)^2 \frac{\gamma_I^2 \mu_{eff}^4 \beta^4 H_0^2}{r_i^6 (3kT)^2}\left(\frac{\tau_r}{1+\omega_I^2\tau_r^2}\right) \quad (5)$$

$$\frac{1}{T_{1i}^{para}} = \frac{C_j}{r_i^6} \quad (6)$$

$$\frac{T_{1i}^{para}(\mathbf{M})}{T_{1i}^{para}(\mathbf{m})} = \left(\frac{r_i(\mathbf{M})}{r_i(\mathbf{m})}\right)^6 \quad (7)$$

$$\frac{1}{T_{1i}^{para}} = \frac{1}{T_{1i}^{exp}} - \frac{1}{T_{1i}^{dia}} \quad (8)$$

Table 5. Longitudinal ^1H NMR relaxation rates (T_{1i}^{exp} [s]) for the complexes $[Ln(L^{15})](ClO_4)_3 \cdot H_2O$ (Ln = La: **11**; Ln = Nd: **12**) in CD_3CN at 298 K and calculated Ln–H distances (r_i [Å]) for H1 and for the aromatic protons H5–H10 in the two isomers of $[Nd(L^{15})](ClO_4)_3 \cdot H_2O$.[a]

	%[b]	H1	H5	H6	H7	H8	H9	H10
11	71 (**M**)	0.216	0.707	0.928	0.797	0.643	1.005	0.560
11	29 (**m**)	0.304	0.715	0.904	0.7604	0.619	1.051	0.629
12	66 (**M**)	0.185	[c]	0.534	0.400	0.140	0.296	0.135
12	34 (**m**)	0.240	[c]	0.572	0.397	0.139	0.293	0.129
r_i(**M**)[d]		6.00	3.91	7.43	7.01	5.54	6.24	5.43
r_i(**m**)[e]		5.88	[c]	7.70	7.05	5.54	6.20	5.35

[a] See Scheme 1 for the numbering scheme. Typical relative errors for T_1 are within 2%. [b] Ratio of the two isomers according to the integration of ^1H NMR signals, **M** and **m**, respectively, are assigned to the major and minor isomers. [c] Masked by aliphatic signals. [d] Taken from the crystal structure of $[La(L^{15})](ClO_4)_3$ (**18**). [e] Calculated with Equations (7) and (8) for the minor isomer.

Taking the Ln–H distances measured in the crystal structure of $[La(L^{15})](ClO_4)_3$ (**18**) as a model for the major isomer (r_i(**M**)) observed for $[Nd(L^{15})]^{3+}$ in solution, the related distances in the minor isomer (r_i(**m**)) have been calculated with Equation (7) and collected in Table 5. Although complicated interpenetrated signals prevent relaxation measurements for H2 and H3, the r_i(**m**) distance obtained for the apical proton H1 shows only a small contraction in the minor isomer (r_i(**M**) – r_i(**m**) = 0.12 Å); this confirms both the exclusive formation of endo isomers in solution and the slight structural change affecting the tripod in the two isomers. This is further exemplified by the 0.27 Å extension observed for H6 when going from **M** to **m**.[39] However, the similar r_i(**m**) and r_i(**M**) values found for the aromatic protons of the tridentate binding units (H7–H10) strongly support the existence of two conformers in solution with comparable coordination spheres and slightly different arrangement of the ethyleneoxy spacers as found in the solid state. The small ΔG values measured in solution implies two well-defined minima in the energy hypersurface explored by the conformations of the tripod. The high activation energy $\Delta G^{\neq}$ estimated for the $\mathbf{M} \rightleftharpoons \mathbf{m}$ process in solution suggests, however, that the conformational interconversion requires the partial decomplexation of the metal.

Photophysical properties of $[Ln(L^{15})](ClO_4)_3 \cdot H_2O$ (Ln = La: 11; Ln = Eu: 13; Ln = Gd: 14; Ln = Tb: 15): The ligand L^{15}

displays a broad and assymmetric absorption band envelope centered at 31650 cm^{-1} in acetonitrile and assigned to the $\pi \rightarrow \pi^*$ transitions , as previously established for L^7.[13a] Upon complexation to Ln^{III} in $[Ln(L^{15})]^{3+}$ (Ln = La, Eu, Gd, Tb), this band is red-shifted by approximately 1350 cm^{-1}; this allows the monitoring of the complexation process by spectrophotometry (Figure 1). A parallel behavior is observed in the solid state (Table 6) and excitation of the ligand-centered transition in L^{15} (solid-state, 77 K, $\lambda_{exc} = 27620\ cm^{-1}$) provides a poorly resolved fluorescence spectrum originating from the $^1\pi\pi^*$ level (0–0 phonon at 24330 cm^{-1}). Time-resolved spectra do not exhibit detectable phosphorescence (delay times: 0.01–100 ms), which points to inefficient intersystem crossing and/or efficient non-radiative quenching of the $^3\pi\pi^*$ state. The complexed ligand in the diamagnetic complex $[La(L^{15})](ClO_4)_3 \cdot H_2O$ (**11**) shows very similar emission spectra (Table 6). For the paramagnetic complex $[Gd(L^{15})](ClO_4)_3 \cdot H_2O$ (**14**), the metal-centered excited levels are too high to be accessible for intramolecular energy transfers from the $^1\pi\pi^*$ or $^3\pi\pi^*$ levels,[40] but the Coulomb interactions between the electrons of the ligands and the metal ion mix the ligand-centered triplet and singlet wavefunctions.[41] Consequently, both the $^1\pi\pi^* \rightarrow {}^3\pi\pi^*$ intersystem crossing (isc) and the radiative emission of the spin-forbidden $^3\pi\pi^*$ level become more efficient.[41] The emission spectrum of **14** at 77 K thus displays the expected $^1\pi\pi^*$ fluorescence at 24390 cm^{-1} together with a weak, but significant $^3\pi\pi^*$ emission at 20370 cm^{-1} (0–0 phonon, vibronic progression $\approx 1000\ cm^{-1}$, Figure 6a). These values slightly differ from those reported for $[GdZn(L^7)_3]^{5+}$ in which Gd^{III} is nine-coordinate in a similar N_6O_3 site ($E(^1\pi\pi^*) = 26600\ cm^{-1}$ and $E(^3\pi\pi^*) = 19960\ cm^{-1}$). The adjacent bidentate binding unit in the segmental ligand L^7 complicates the interpretation of the photophysical properties and prevents closer comparisons.[13a] The ligand-centered luminescence in $[Eu(L^{15})](ClO_4)_3 \cdot H_2O$ (**13**) and $[Tb(L^{15})](ClO_4)_3 \cdot H_2O$ (**15**) is partially quenched by $L^{15} \rightarrow Ln^{III}$ energy-transfer processes. Excitation by means of the ligand-centered $\pi \rightarrow \pi^*$ transitions produces faint residual emission of the $^1\pi\pi^*$ (Ln = Eu, Tb) and $^3\pi\pi^*$ (Ln = Eu) levels. Also seen is a strong metal-centered luminescence characterized by sharp bands associated with $^5D_0 \rightarrow {}^7F_j$ ($j = 0-6$) for **13** and $^5D_4 \rightarrow {}^7F_j$ ($j = 6-0$) for **15** (Figure 6b and c). Detailed high-resolution emission studies in the solid state are in progress and the discussion of symmetry site, crystal-field and nephelauxetic parameters, and excited-state lifetimes in the solid-state will be published elsewhere.[10] However, the observation of residual $^1\pi\pi^*$ emission for the coordinated ligand in $[Eu(L^{15})](ClO_4)_3 \cdot H_2O$ (**13**) and $[Tb(L^{15})](ClO_4)_3 \cdot H_2O$ (**15**) points to inefficient $L^{15} \rightarrow Ln^{III}$ (Ln = Eu, Tb) energy-transfer processes. This behavior is confirmed by the concomittant observation of faint emission of the ligand-centered triplet state in **13**.

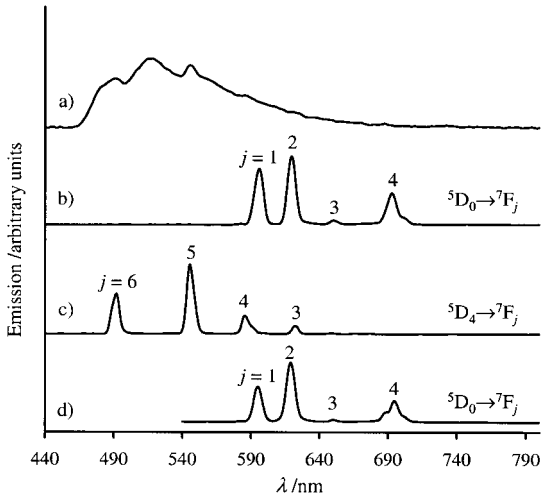

Figure 6. Time-resolved phosphorescence spectra (delay 0.1 ms) of a) $[Gd(L^{15})](ClO_4)_3 \cdot H_2O$ (**14**, $\lambda_{exc} = 27030\ cm^{-1}$, 77 K), b) $[Eu(L^{15})](ClO_4)_3 \cdot H_2O$ (**13**, $\lambda_{exc} = 27170\ cm^{-1}$, 77 K), c) $[Tb(L^{15})](ClO_4)_3 \cdot H_2O$ (**15**, $\lambda_{exc} = 27397\ cm^{-1}$, 77 K), and d) $[Eu(L^{15})]^{3+}$ in acetonitrile (10^{-3} mol dm^{-3}, $\lambda_{exc} = 26385\ cm^{-1}$, 298 K).

The emission spectra of the podates $[Eu(L^{15})]^{3+}$ and $[Tb(L^{15})]^{3+}$ in acetonitrile (10^{-3} mol dm^{-3}, 293 K) closely match those obtained in the solid state, in agreement with the preservation of the C_3-symmetrical structure in solution previously demonstrated by NMR spectroscopy. The $Eu(^5D_0)$ and $Tb(^5D_4)$ lifetimes measured upon irradiation of the ligand-centered levels amount to 2.58(3) ms ($\lambda_{exc} = 26385\ cm^{-1}$) and 0.019(1) ms ($\lambda_{exc} = 26455\ cm^{-1}$), respectively. The long lifetime obtained for $[Eu(L^{15})]^{3+}$ is diagnostic for the absence of high-frequency oscillators in the first coordination sphere,[24] implying that no solvent molecule is bound to the metal in solution. Moreover, the spectral characteristics in solution are very similar to those previously reported for $[EuZn(L^7)_3]^{5+}$ ($\tau Eu(^5D_0) = 2.56(2)$ ms),[13a] thus pointing to similar pseudo-tricapped trigonal prismatic N_6O_3 coordination spheres in solution. The absolute quantum yield is modest ($\Phi_{Eu} = 4.3 \times 10^{-3}$) and reflects the poor efficiency of intersystem crossing and energy-transfer processes. It is, however, more than twice that reported for $[EuZn(L^7)_3]^{5+}$.[13a] For

Table 6. Ligand-centered absorption and emission properties for the ligand L^{15} and its complexes $[Ln(L^{15})_3](ClO_4)_3 \cdot H_2O$ (Ln = La: **11**; Ln = Eu: **13**; Ln = Gd: **14**; Ln = Tb: **15**).[a]

	$E(\pi \rightarrow \pi^*)$ [cm^{-1}][b] Absorption	$E(\pi \rightarrow \pi^*)$ [cm^{-1}] Absorption	$E(^1\pi\pi^*)$ [cm^{-1}] Emission	$E(^3\pi\pi^*)$ [cm^{-1}] Emission
L^{15}	31650 (59540)	31050	24330 sh, 22220, 20535 sh	[c]
$[La(L^{15})_3]^{3+}$	30300 (49390)	30390	24155	[c]
$[Gd(L^{15})_3]^{3+}$	30300 (47870)	29670	24390, 22420, 20370	20370, 19305, 18315
$[Eu(L^{15})_3]^{3+}$	30300 (47420)	30870	24000 sh, 22700	20280
$[Tb(L^{15})_3]^{3+}$	30210 (50660)	31450	23800 sh, 22400	[d]

[a] Solid-state reflectance spectra and transmission solution spectra recorded at 295 K, luminescence data on solid-state sample at 77 K; sh = shoulder. [b] 10^{-4} mol dm^{-3} in acetonitrile. [c] Not detected. [d] $^3\pi\pi^*$ luminescence quenched by transfer to Ln^{III} ion.

0947-6539/03/0905-1070 $ 20.00+.50/0 *Chem. Eur. J.* **2003**, *9*, No. 5

$[Tb(L^{15})]^{3+}$, the lifetime is dramatically short as a result of the resonant positions of the ligand-centered $^3\pi\pi^*$ (20370 cm^{-1}, Table 6) and $Tb(^5D_4)$ (20325 cm^{-1}, Figure 6c) levels; this induces efficient $Tb \rightarrow$ ligand energy back-transfer.[42] The associated quantum yield is consequently very low ($\Phi_{Tb} = 1.4 \times 10^{-3}$), but again slightly better than that reported for $[TbZn(L^7)_3]^{5+}$, for which the emission intensity was too weak to be measured.[13a] We conclude that the replacement of the noncovalent [Zn(α,α′-diimime)$_3$] tripod in $[LnZn(L^7)_3]^{5+}$ with a semirigid covalent tripod in $[Ln(L^{15})]^{3+}$ has negligible effects on the photophysical properties of the ligand-centered excited states associated with the tridentate binding units. The luminescent behaviors of Eu^{III} and Tb^{III} coordinated in the nine-coordinate metallic sites is also scarcely effected.

Conclusion

The seven-atom mixed aliphatic-aromatic spacers separating the tridentate binding units from the capping atom in the tripod of $[Ln(L^{15})]^{3+}$ represent a compromise between the regular helical wrapping of the strands, ensured by the rigid aromatic eight-atom spacers in the noncovalent tripods of $[LnM(L^7)_3]^{5/6+}$ ($M = Zn^{II}$,[13a] $M = Co^{III}$[13c]), and the flexible aliphatic four-atom TREN tripods in $[Ln(L^{10})]^{3+}$[17] and five-atom TRPN tripods in $[Ln(L^{12})]^{3+}$.[19] The irregular wrapping and fast dynamic behavior of the three strands in the two last complexes is removed by the introduction of aromatic segments within the spacers of the tripod, and the selective formation of stable podates $[Ln(L^{15})]^{3+}$ in solution results from a delicate balance between rigidity and flexibility. This allows the regular wrapping of the strands required for the complexation of large metal ions in pseudo-tricapped trigonal prismatic sites. However, the formation of two different conformers, depending on the precise arrangement of the aliphatic part of the tripod, indicates that structural programming is not perfect in $[Ln(L^{15})]^{3+}$. It also suggests that a larger free-energy gap between the possible conformers of the tripod is required to design an universal tripod for lanthanide-containing, trigonal, nine-coordinate podates. Our detailed investigations in the solid-state and in solution demonstrate that the two conformers of $[Ln(L^{15})]^{3+}$ display only minor structural variations and possess similar ground-state energies. The kinetic barrier for their interconversion is, however, considerable because it requires the partial decomplexation of the metal. Further work aiming at the rational increases of ΔG between the possible conformers for producing a single isomer is currently under investigation.

Experimental Section

Solvents and starting materials: These were purchased from Fluka AG (Buchs, Switzerland) and used without further purification unless otherwise stated. Thionyl chloride was distilled with elemental sulfur. Acetonitrile, dichloromethane, *N,N*-dimethyformamide, and triethylamine were distilled with CaH_2. Silicagel (Acros, 0.035–0.07 mm) was used for preparative column chromatography. *N*-ethyl-(4-methoxymethyl-2-nitrophenyl)amine (**2**),[26] 6-(*N,N*-diethylcarbamoyl)pyridine-2-carboxylic acid (**3**),[25] and 3-(2-hydroxyethyl)pentane-1,5-diol (**10**)[28] were prepared according to literature procedures. The triflate salts $Ln(CF_3SO_3)_3 \cdot nH_2O$ (Ln = La–Lu) and the perchlorate salts $Ln(ClO_4)_3 \cdot nH_2O$ (Ln = La–Lu) were prepared from the corresponding oxides (Rhodia, 99.99%) and dried according to published procedures.[43] The Ln content of solid salts was determined by complexometric titrations with Titriplex III (Merck) in the presence of urotropine and xylene orange.[44]

Caution: Dry perchlorates may explode and should be handled in small quantities and with the necessary precautions.[45]

Preparation of compound 4: A mixture of **3** (9.33 g, 42 mmol), CH_2Cl_2 (120 mL), thionyl chloride (30.6 mL, 420 mmol), and DMF (0.1 mL) was refluxed for 1.5 h under a nitrogen atmosphere and evaporated to dryness. The white residue was dried under vacuum for 30 min, dissolved in CH_2Cl_2 (60 mL), and cooled to 0 °C. A mixture of **2** (7.36 g, 35 mmol), triethylamine (25 mL), and CH_2Cl_2 (50 mL) was added dropwise. The resulting solution was stirred for 10 min at 0 °C, refluxed for 2 h, and evaporated to dryness. The residual brown oil was dissolved in CH_2Cl_2/aqueous half-saturated NH_4Cl (200 mL/300 mL), the organic layer was separated, and the aqueous layer was extracted with CH_2Cl_2 (4 × 25 mL). The combined organic phases were washed with deionized water (50 mL), dried over $MgSO_4$, filtered, and evaporated to dryness. The resulting crude compound was purified by column chromatography (silicagel, CH_2Cl_2/MeOH 99:1 → 96:4) to afford **4** as a brown oil (12.28 g, 29.6 mmol, 85%). ^1H NMR ($CDCl_3$): $\delta = 0.91$ (t, $^3J = 7.2$ Hz, 3H; CH_3(amide)), 1.20 (t, $^3J = 7.2$ Hz, 3H; CH_3(amide)), 1.25 (t, $^3J = 7.2$ Hz, 3H; CH_3(amide)), 2.96 (sext, $^2J = 14.4$, $^3J = 7.2$ Hz, 1H; CH_2(amide)), 3.32 (sext, $^2J = 14.4$, $^3J = 7.2$ Hz, 1H; CH_2(amide)), 3.40 (s, 3H; CH_3), 3.51 (sext, $^2J = 14.4$, $^3J = 7.2$ Hz, 1H; CH_2(amide)), 3.60 (sext, $^2J = 14.4$, $^3J = 7.2$ Hz, 1H; CH_2(amide)), 4.32 (sext, $^2J = 14.4$, $^3J = 7.2$ Hz, 1H; CH_2(amide)), 4.45 (s, 2H; CH_2), 7.17 (d, $^3J = 7.8$ Hz, 1H; CH), 7.33 (dd, $^3J = 7.5$, $^4J = 1.2$ Hz, 1H; CH), 7.43 (dd, $^3J = 8.4$, $^4J = 1.2$ Hz, 1H; CH), 7.77 (d, $^3J = 7.8$ Hz, 1H; CH), 7.82 (dd, $^3J = 8.1$, $^4J = 1.5$ Hz, 1H; CH), 7.93 ppm (d, $^4J = 1.8$ Hz, 1H; CH); ^{13}C NMR ($CDCl_3$): $\delta = 12.4$, 12.6, 14.0, 39.8, 42.6, 45.9, 58.5, 72.6, 123.5, 123.9, 124.5, 131.8, 132.0, 135.7, 137.2, 139.8, 146.1, 151.3, 152.9, 166.3, 167.3 ppm; IR (KBr): $\tilde{\nu} = 3070$, 2980, 2940, 2880, 1640, 1570, 1530, 1485 cm^{-1}; EI-MS: *m/z* (%): 415 (5) [M^+], 368 (17) [$M^+ - HNO_2$], 343 (27) [$M^+ - NEt_2$], 316 (13) [$M^+ - CONEt_2$+H], 72 (100) [NEt_2].

Preparation of compound 5: A mixture of **4** (4.86 g, 11.7 mmol), ethanol (420 mL), water (120 mL), powdered iron (5.24 g, 93.6 mmol), and concentrated hydrochloric acid (37%, 14 mL, 168.5 mmol) was refluxed for 18 h under a nitrogen atmosphere, filtered, and concentrated under vacuum. The residual aqueous layer was poured into a mixture of CH_2Cl_2 (200 mL), water (370 mL) and $Na_2H_2EDTA \cdot 2H_2O$ (63.2 g, 169.6 mmol). The pH was adjusted to 7 with a 25% aqueous ammonia solution, 30% hydrogen peroxide solution (3.5 mL, 34.4 mmol) was slowly added, and the mixture was stirred for 15 min. The pH was adjusted to 8.5 with a 25% aqueous ammonia solution, the aqueous layer was extracted with CH_2Cl_2 (3 × 50 mL), and the combined organic layers were washed with deionized water until neutral, dried over $MgSO_4$, filtered, and evaporated to dryness. The resulting crude compound was purified by column chromatography (silicagel, CH_2Cl_2/MeOH 98:2) to afford **5** as a pale yellow solid (4.01 g, 10.96 mmol, 93%). ^1H NMR ($CDCl_3$): $\delta = 1.07$ (t, $^3J = 7.2$ Hz, 3H; CH_3(amide)), 1.29 (t, $^3J = 7.2$ Hz, 3H; CH_3(amide)), 1.48 (t, $^3J = 7.2$ Hz, 3H; CH_3(Et)), 3.35 (q, $^3J = 7.2$ Hz, 2H; CH_2(amide)), 3.40 (s, 3H; CH_3), 3.62 (q, $^3J = 7.2$ Hz, 2H; CH_2(amide)), 4.61 (s, 2H; CH_2), 4.78 (q, $^3J = 7.2$ Hz, 2H; CH_2(Et)), 7.39 (dd, $J = 8.4$, $^3J = 1.2$ Hz, 1H; CH), 7.46 (d, $^3J = 8.4$ Hz, 1H; CH), 7.57 (dd, $^3J = 7.6$, $^4J = 1.2$ Hz, 1H; CH), 7.81 (s, 1H; CH), 7.97 (t, $^3J = 7.9$ Hz, 1H; CH), 8.45 ppm (d, $^3J = 7.5$ Hz, 1H; CH); ^{13}C NMR ($CDCl_3$): $\delta = 12.8$, 14.3, 15.4, 39.5, 40.6, 42.8, 57.8, 75.1, 110.1, 119.7, 122.5, 123.9, 125.0, 132.9, 135.9, 138.0, 142.7, 149.4, 149.6, 154.5, 168.4 ppm; IR (KBr): $\tilde{\nu} = 3050$, 2980, 2940, 2880, 2820, 1715, 1635, 1570, 1485 cm^{-1}; EI-MS: *m/z* (%): 366 (23) [M^+], 335 (3) [$M^+ - OCH_3$], 267 (100) [$M^+ - CONEt_2$+H].

Preparation of compound 6: A mixture of **5** (990 mg, 2.70 mmol), acetic anhydride (20 mL), and $BF_3 \cdot Et_2O$ (3.8 mL, 30.0 mmol) was stirred at room temperature (25 °C) for 1 h and poured into an ice-cooled aqueous 2 M KOH (500 mL). The aqueous layer was extracted with CH_2Cl_2 (4 × 50 mL). The combined organic layers were washed with deionized water until neutral, dried over $MgSO_4$, filtered, and evaporated to dryness to afford the crude acetate as a pale yellow solid (1065 mg, 100%), which was dissolved in methanol (50 mL) and 1 M KOH aqueous solution (50 mL), stirred for 15 h at room temperature, concentrated under vacuum, poured into brine

(500 mL), and extracted with CH_2Cl_2 (7×50 mL). The combined organic layers were washed with deionized water until neutral, dried over $MgSO_4$, filtered, and evaporated to dryness. The resulting crude compound was purified by column chromatography (silicagel, CH_2Cl_2/MeOH 95:5) to afford **6** as a white solide (896 mg, 2.55 mmol, 94%). ^{1}H NMR ($CDCl_3$): $\delta = 1.07$ (t, $^3J = 7.2$ Hz, 3H; CH_3(amide)), 1.29 (t, $^3J = 7.2$ Hz, 3H; CH_3 (amide)), 1.46 (t, $^3J = 7.2$ Hz, 3H; (CH_3(Et)), 2.21 (brs, 1H; OH), 3.35 (q, $^3J = 7.2$ Hz, 2H; CH_2(amide)), 3.61 (q, $^3J = 7.2$ Hz, 2H; CH_2(amide)), 4.75 (^3J, $J = 7.2$ Hz, 2H; CH_2(Et)), 4.81 (s, 2H; CH_2), 7.37 (dd, $^3J = 9.3$, $^4J = 1.5$ Hz, 1H; CH), 7.43 (d, $^3J = 8.4$ Hz, 1H; CH), 7.55 (dd, $^3J = 7.8$, $^4J = 1.1$ Hz, 1H; CH), 7.79 (s, 1H; CH), 7.94 (t, $^3J = 8.1$ Hz, 1H; CH), 8.39 ppm (dd, $^3J = 8.1$, $^4J = 1.1$ Hz, 1H; CH); ^{13}C NMR ($CDCl_3$): $\delta = 12.9$, 14.4, 15.5, 39.7, 40.8, 42.9, 65.8, 110.3, 118.8, 122.7, 123.5, 125.2, 135.8, 136.2, 138.2, 142.7, 149.3, 149.7, 154.6, 168.6 ppm; EI-MS: m/z (%): 352 (29) [M^+], 281 (6) [$M^+ - NEt_2$+H], 253 (100) [$M^+ - CONEt_2$+H].

Preparation of compound 7: A mixture of **6** (705 mg, 2.0 mmol), CH_2Cl_2 (20 mL), and thionyl chloride (1.46 mL, 20.0 mmol) was stirred at 0 °C for 30 min and at room temperature (25 °C) for 4 h; it was then poured into a $NaHCO_3$-saturated aqueous solution (250 mL). The aqueous layer was extracted with CH_2Cl_2 (2×10 mL). The combined organic layers were washed with deionized water until neutral, dried over $MgSO_4$, filtered, and evaporated to dryness. The resulting crude compound was purified by column chromatography (silicagel, CH_2Cl_2/MeOH 96:4) to afford **7** as a white solid (725 mg, 1.96 mmol, 98%). ^{1}H NMR ($CDCl_3$): 1.05 (t, $^3J = 7.0$ Hz, 3H; CH_3(amide)), 1.26 (t, $^3J = 7.2$ Hz, 3H; CH_3(amide)), 1.46 (t, $^3J = 7.2$ Hz, 3H; CH_3(Et)), 3.32 (q, $^3J = 7.0$ Hz, 2H; CH_2(amide)), 3.59 (q, $^3J = 7.2$ Hz, 2H; CH_2(amide)), 4.75 (s, 2H; CH_2Cl), 4.76 (q, $^3J = 7.1$ Hz, 2H; CH_2(amide)), 7.41 (d, $^3J = 9.0$ Hz, 1H; CH), 7.46 (d, $^3J = 8.4$ Hz, 1H; CH), 7.56 (d, $^3J = 7.5$ Hz, 1H; CH), 7.87 (s, 1H; CH), 7.96 (t, $^3J = 8.0$ Hz, 1H; CH), 8.45 ppm (d, $^3J = 8.1$ Hz, 1H; CH); ^{13}C NMR ($CDCl_3$): 13.2, 14.6, 15.7, 39.9, 41.1, 43.1, 47.5, 110.9, 120.6, 123.1, 125.0, 125.5, 132.8, 136.4, 138.5, 142.5, 149.2, 150.3, 154.9, 168.7 ppm; EI-MS: m/z (%): 370 (21) [M^+], 335 (8) [$M^+ -$ Cl], 271 (100) [$M^+ - CONEt_2$+H].

Preparation of ligand L[15]: A solution of **10** (30 mg, 0.20 mmol) in DMF (2 mL) was added to a suspension of NaH (60% dispersion in mineral oil, 32 mg, 0.80 mmol) in dry DMF (2 mL). After 30 min of stirring at room temperature (25 °C), a solution of **7** (260 mg, 0.70 mmol) in DMF (3 mL) was added. The mixture was stirred at room temperature for 15 h and poured into brine (200 mL). The solution was extracted with CH_2Cl_2 ($4 \times$ 20 mL). The combined organic layers were washed with deionized water until neutral, dried over $MgSO_4$, filtered, and evaporated to dryness. The resulting crude compound was purified by column chromatography (silicagel, CH_2Cl_2/MeOH 95:5) to afford pure $L^{15} \cdot H_2O$ as a white solid (171 mg, 0.146 mmol, 73%). ^{1}H NMR ($CDCl_3$): $\delta = 1.05$ (t, $^3J = 7.2$ Hz, 9H; CH_3(amide)), 1.27 (t, $^3J = 7.2$ Hz, 9H; CH_3(amide)), 1.43 (t, $^3J = 7.2$ Hz, 9H; CH_3(Et)), 1.64 (q, $^3J = 6.7$ Hz, 6H; HC–CH_2–CH_2,), 1.80 (hept, $^3J = 6.2$ Hz, 1H; H1), 3.34 (q, $^3J = 7.1$ Hz, 6H; CH_2(amide)), 3.52 (t, $^3J = 6.9$ Hz, 6H; HC–CH_2–CH_2), 3.60 (q, $^3J = 7.1$ Hz, 6H; CH_2(amide)), 4.60 (s, 6H; CH_2), 4.74 (q, $^3J = 7.2$ Hz, 6H; CH_2(Et)), 7.33 (dd, $^3J = 8.4$, $^4J = 1.2$ Hz, 3H; CH), 7.40 (d, $^3J = 8.7$ Hz, 3H; CH), 7.54 (dd, $^3J = 8.4$, $^4J = 0.8$ Hz, 3H; CH), 7.76 (s, 3H; CH), 7.92 (t, $^3J = 7.8$ Hz, 3H; CH), 8.37 ppm (dd, $^3J = 7.8$, $^4J = 0.8$ Hz, 3H; CH); ^{13}C NMR ($CDCl_3$): $\delta = 13.1$, 14.6, 15.7, 29.8, 34.2, 39.8, 40.9, 43.1, 68.5, 73.7, 110.4, 119.8, 122.8, 124.1, 125.3, 133.6, 136.1, 138.3, 143.0, 149.7, 149.9, 154.7, 168.8 ppm; ESI-MS (CH_2Cl_2): 1152 [M^++H]; elemental analysis calcd (%) for $C_{67}H_{84}N_{12}O_7$: C 68.81, N 14.37, H 7.24; found: C 68.73, N 14.01, H 7.29.

Preparation of the complexes $[Ln(L^{15})](ClO_4)_3 \cdot nH_2O$ (Ln = La, $n = 1$: 11; Ln = Nd, $n = 1$: 12; Ln = Eu, $n = 1$: 13; Ln = Gd, $n = 1$: 14; Ln = Tb, $n = 1$: 15; Ln = Lu, $n = 4$: 16; Ln = Y, $n = 1$: 17): A solution of $Ln(ClO_4)_3 \cdot nH_2O$ (Ln = La, Nd, Eu, Gd, Tb, Lu, Y; 0.017 mmol) in acetonitrile (3 mL) was added to a solution of $L^{15} \cdot H_2O$ (20.0 mg, 0.017 mmol) in acetonitrile (3 mL). Diethyl ether was diffused into the solution for 1 day. The resulting white microcrystalline powders were collected by filtration and dried to give 72–93% of $[Ln(L^{15})](ClO_4)_3 \cdot nH_2O$ (Ln = La, $n = 1$: **11**; Ln = Nd, $n = 1$: **12**; Ln = Eu, $n = 1$: **13**; Ln = Gd, $n = 1$: **14**; Ln = Tb, $n = 1$: **15**; Ln = Lu, $n = 4$: **16**; Ln = Y, $n = 1$: **17**). All of these complexes were characterized by their IR spectra and gave satisfying analyses (Table S2, Supporting Information). Fragile monocrystals suitable for X-ray diffraction studies were obtained for $[Ln(L^{15})](ClO_4)_3$ (Ln = La, Eu) upon ultra-slow diffusion of diethyl ether into concentrated acetonitrile solutions.

Crystal structure determination of $[Ln(L^{15})](ClO_4)_3$ (Ln = La, 18; Ln = Eu, 19): Crystal structure determination of $[La(L^{15})](ClO_4)_3$ (**18**) and unit cell parameters (between brackets) for the isostructural $[Eu(L^{15})](ClO_4)_3$ (**19**) complex: $LaCH(C_{22}H_{27}N_4O_3)_3(ClO_4)_3$: $M_r = 1588.9$; $\mu = 0.79$ mm^{-1}, $\rho_{calcd} = 1.478$ g cm^{-3}, trigonal, $R3c$, $Z = 6$, $a = 22.1077(10)$ [21.9972(11)], $c = 25.2974(11)$ Å [25.4375(4)], $V = 10708(1)$ Å^3 [10660(1)]; colorless prism $0.13 \times 0.14 \times 0.32$ mm mounted on a quartz fiber with protection oil. Cell dimensions and intensities were measured at 200 K on a Stoe IPDS diffractometer with graphite-monochromated $Mo_{K\alpha}$ radiation ($\lambda = 1.5418$ Å); 45188 measured reflections, $2\theta_{max} = 52°$, 4632 unique reflections of wich 3241 were observables ($|F_o| > 4\sigma(F_o)$); R_{int} for 38948 equivalent reflections 0.054. Data were corrected for Lorentz and polarization effects and for absorption (min/max transmission = 0.8590, 0.9261). The structure was solved by direct methods (SIR97),[46] and all other calculation were performed with XTAL[47] system and ORTEP[48] programs. Full-matrix least-squares refinement based on F by using a weight of $1/(\sigma^2(F_o) + 0.00055(F_o^2))$ gave final values $R = 0.032$, $\omega R = 0.039$ and $S = 1.89(4)$ for 340 variables and 3241 contributing reflections. Flack parameter $x = -0.02(3)$. The final difference electron density map showed a maximum of $+0.43$ and a minimum of -0.47 e Å^{-3}. The hydrogen atoms were placed in calculated positions and contributed to F_c calculations. The C2, C3, and O1 atoms were disordered and refined with two distinct atomic sites for each atom and population parameters of 0.8/0.2, thus leading to two different conformations of the ethyleneoxy spacers of the tripods. The minor conformation was refined with isotropic displacement parameters and restraints on bond distances and bond angles. The major conformation was refined with anisotropic displacement parameters (Figure S2, Supporting Information). The perchlorate anion was fully disordered and refined with two atomic sites for the chlorine atom and nine sites for the oxygen atoms.

CCDC-192 826 contains the supplementary crystallographic data for $La(L^{15})(ClO_4)_3$ (**18**). These data can be obtained free of charge at www.ccdc.cam.ac.uk/conts/retrieving.html (or from the Cambridge Crystallographic Data Centre, 12 Union Road, Cambridge CB2 1EZ, UK; fax: (+44) 1223–336–033; or deposit@ccdc.cam.ac.uk).

Spectroscopic and analytical measurements: Reflectance spectra were recorded as finely ground powders dispersed in MgO (5%) with MgO as reference on a Perkin–Elmer Lambda 900 spectrophotometer equipped with a PELA-1020 integrating sphere from Labsphere. Electronic spectra in the UV-visible region were recorded at 20 °C from 10^{-4} mol dm^{-3} solutions in MeCN with a Perkin–Elmer Lambda 900 spectrometer by using quartz cells of 0.1 and 1 cm path length. Spectrophotometric titrations were performed with a J&M diode array spectrometer (Tidas series) connected to an external computer. In a typical experiment, 50 mL of $L^{15} \cdot H_2O$ in acetonitrile (10^{-4} mol dm^{-3} + 0.01 mol dm^{-3} [N(nBu)$_4$]ClO$_4$) were titrated at 20 °C with an equimolar solution of $Ln(ClO_4)_3 \cdot nH_2O$ (10^{-3} mol dm^{-3}) in acetonitrile under an N_2 atmosphere. After each addition of 0.10 mL, the absorbances were recorded using Hellma optrodes (optical path length 0.1 and 0.5 cm) immersed in the thermostated titration vessel and connected to the spectrometer. Mathematical treatment of the spectrophotometric titrations was performed with factor analysis[49] and with the SPECFIT program.[29] IR spectra were obtained from KBr pellets with a Perkin–Elmer 883 spectrometer. ^{1}H and ^{13}C NMR spectra were recorded at 25 °C on a Broadband Varian Gemini 300 spectrometer. Chemical shifts are given in ppm with respect to TMS. The determination of longitudinal relaxation times (T_1) used the inversion-recovery technique. EI-MS (70 eV) were recorded with a VG-7000E instrument. Pneumatically-assisted electrospray (ESI-MS) mass spectra were recorded from 10^{-4} mol dm^{-3} acetonitrile solutions on a Finnigan SSQ 7000 instrument. Excitation and emission spectra as well as lifetime measurements were recorded on a Perkin–Elmer LS-50B spectrometer equipped for low-temperature measurements.

The quantum yields Φ were calculated by using Equation (9), in which x refers to the sample and r to the reference; A is the absorbance, ν the

$$\frac{\Phi_x}{\Phi_r} = \frac{A_r(\tilde{\nu})\, I_r(\tilde{\nu})\, n_x^2\, D_x}{A_x(\tilde{\nu})\, I_x(\tilde{\nu})\, n_r^2\, D_r} \qquad (9)$$

excitation wavenumber used, I the intensity of the excitation light at this energy, n the refractive index, and D the integrated emitted intensity. $[Eu(terpy)_3](ClO_4)_3$ ($\Phi = 1.3\%$, acetonitrile, 10^{-3} mol dm^{-3}) and $[Tb(terpy)_3](ClO_4)_3$ ($\Phi = 4.7\%$, acetonitrile, 10^{-3} mol dm^{-3}) were used as

0947-6539/03/0905-1072 $ 20.00+.50/0 *Chem. Eur. J.* **2003**, *9*, No. 5

references for the determination of quantum yields of respectively Eu- and Tb-containing samples.[5b, 33] Elemental analyses were performed by Dr. H. Eder from the Microchemical Laboratory of the University of Geneva.

Acknowledgement

This work is supported through grants from the Swiss National Science Foundation.

[1] A. J. Freeman, R. E. Watson, *Phys. Rev. B.* **1962**, *127*, 2058.

[2] J.-C. G. Bünzli, in *Rare Earths* (Eds.: R. Saez Puche, P. Caro), Editorial Complutense S. A., Madrid, **1998**, pp. 223–259.

[3] J.-C. G. Bünzli, C. Piguet, *Chem. Rev.* **2002**, *102*, 1897.

[4] a) A. Abragam, B. Bleaney, *Electron Paramagnetic Resonance of Transitions Ions*, Clarendon, Oxford, **1970**; b) W. T. Carnall, in *Handbook on the Physics and Chemistry of Rare Earths* (Eds.: K. A. Gschneidner, L. Eyring), North-Holland, Amsterdam, **1979**, pp. 171–208; c) C. Görrler-Walrand, K. Binnemans, in *Handbook on the Physics and Chemistry of Rare Earths, Vol. 23* (Eds.: K. A. Gschneidner, L. Eyring), North-Holland, Amsterdam, **1996**, pp. 121–283; d) P. Porcher, in *Rare Earths* (Eds.: R. Saez Puche, P. Caro), Editorial Complutense S. A., Madrid, **1998**, pp. 43–66.

[5] a) R. T. Wegh, H. Donker, K. D. Oskam, A. Meijerink, *J. Lumin.* **1999**, *82*, 93; b) S. Petoud, J.-C. G. Bünzli, C. Piguet, Q. Xiang, R. Thummel, *J. Lumin.* **1999**, *82*, 69; c) S. Heer, M. Wermuth, K. Krämer, D. Ehrentraut, H. U. Güdel, *J. Lumin.* **2001**, *94–95*, 337; d) C. Reinhard, H. U. Güdel, *Inorg. Chem.* **2002**, *41*, 1048.

[6] a) M. H. V. Werts, J. W. Verhoeven, J. W. Hofstraat, *J. Chem. Soc. Perkin Trans. 2* **2000**, 433; b) G. F. de Sa, O. L. Malta, C. de Mello Donega, A. M. Simas, R. L. Longo, P. A. Santa-Cruz, E. F. da Silva, Jr, *Coord. Chem. Rev.* **2000**, *196*, 165; c) A. Beeby, L. M. Bushby, D. Maffeo, J. A. G. Williams, *J. Chem. Soc. Dalton Trans.* **2002**, 48.

[7] a) V. S. Mironov, Y. G. Galyametdinov, A. Ceulemans, K. Binnemans, *J. Chem. Phys.* **2000**, *113*, 10293; b) I. Bertini, M. B. L. Janik, Y.-M. Lee, C. Luchinat, A. Rosato, *J. Am. Chem. Soc.* **2001**, *123*, 4181; c) V. S. Mironov, Y. G. Galyametdinov, A. Ceulemans, C. Görller-Walrand, K. Binnemans, *J. Chem. Phys.* **2002**, *116*, 4673; d) P. Bernardo, R. Barbieri, E. Padros, C. Luchinat, M. Pons, *J. Am. Chem. Soc.* **2002**, *124*, 374.

[8] J.-C. G. Bünzli, A. Milicic-Tang, in *Handbook on the Physics and Chemistry of Rare Earths*, *Vol. 21* (Eds.: K. A. Gschneidner, L. Eyring), Elsevier, Amsterdam, **1995**, p. 305.

[9] a) F. Renaud, C. Piguet, G. Bernardinelli, J.-C. G. Bünzli, G. Hopfgartner, *Chem. Eur. J.* **1997**, *3*, 1646; b) D. A. Bardwell, J. C. Jeffery, P. L. Jones, J. A. McCleverty, E. Psillakis, Z. Reeves, M. D. Ward, *J. Chem. Soc. Dalton Trans.* **1997**, 2079; c) S. Petoud, J.-C. G. Bünzli, F. Renaud, C. Piguet, K. J. Schenk, G. Hopfgartner, *Inorg. Chem.* **1997**, *36*, 5750; d) H.-R. Mürner, E. Chassat, R. P. Thummel, J.-C. G. Bünzli, *J. Chem. Soc. Dalton Trans.* **2000**, 2809; e) L. I. Semenova, A. N. Sobolev, B. W. Skelton, A. H. White, *Aust. J. Chem.* **1999**, *52*, 519; f) N. Ouali, B. Bocquet, S. Rigault, P.-Y. Morgantini, J. Weber, C. Piguet, *Inorg. Chem.* **2002**, *41*, 1436.

[10] T. LeBorgne, N. André, J.-C. G. Bünzli, G. Bernardinelli, C. Piguet unpublished results.

[11] a) J. Xu, S. J. Franklin, D. W. Whisenhunt, K. N. Raymond, *J. Am. Chem. Soc.* **1995**, *117*, 7245; b) A. R. Johnson, B. O'Sullivan, K. N. Raymond, *Inorg. Chem.* **2000**, *39*, 2652; c) C. J. Sunderland, M. Botta, S. Aime, K. N. Raymond, *Inorg. Chem.* **2001**, *40*, 6746; d) A. Bismondo, P. Di Bernardo, R. Portanova, M. Tolazzi, P. L. Zanonato, *Polyhedron* **2002**, *21*, 1393.

[12] a) A. J. Blake, D. M. J. Doble, W.-S. Li, M. Schröder, *J. Chem. Soc. Dalton Trans.* **1997**, 3655; b) R. Wietzke, M. Mazzanti, J.-M. Latour, J. Pécaut, *J. Chem. Soc. Dalton Trans.* **1998**, 4087; c) B. M. Flanagan, P. V. Bernhardt, E. R. Krausz, S. R. Lüthi, M. J. Riley, *Inorg. Chem.* **2001**, *40*, 5401; d) Y. Bretonnière, M. Mazzanti, J. Pécaut, F. A. Dunand, A. E. Merbach, *Inorg. Chem.* **2001**, *40*, 6737.

[13] a) C. Piguet, J.-C. G. Bünzli, G. Bernardinelli, G. Hopfgartner, S. Petoud, O. Schaad, *J. Am. Chem. Soc.* **1996**, *118*, 6681; b) C. Piguet, E. Rivara-Minten, G. Bernardinelli, J.-C. G. Bünzli, G. Hopfgartner, *J. Chem. Soc. Dalton Trans.* **1997**, 421; c) S. Rigault, C. Piguet, G. Bernardinelli, G. Hopfgartner, *J. Chem. Soc. Dalton Trans.* **2000**, 4587.

[14] J.-M. Lehn, *Chem. Eur. J.* **1999**, *5*, 2455.

[15] S. J. Archibald, A. J. Blake, S. Parsons, M. Schröder, R. E. P. Winpenny, *J. Chem. Soc. Dalton Trans.* **1997**, 173.

[16] J.-P. Costes, A. Dupuis, G. Commenges, S. Lagrave, J.-P. Laurent, *Inorg. Chim. Acta* **1999**, *285*, 49.

[17] F. Renaud, C. Piguet, G. Bernardinelli, J.-C. G. Bünzli, G. Hopfgartner, *J. Am. Chem. Soc.* **1999**, *121*, 9326.

[18] Y. Bretonnière, R. Wietzke, C. Lebrun, M. Mazzanti, J. Pécaut, *Inorg. Chem.* **2000**, *39*, 3499.

[19] F. Renaud, C. Decurnex, C. Piguet, G. Hopfgartner, *J. Chem. Soc. Dalton Trans.* **2001**, 1863.

[20] L. Tei, G. Baum, A. J. Blake, D. Fenske, M. Schröder, *J. Chem. Soc. Dalton Trans.* **2000**, 2793.

[21] L. J. Charbonnière, R. Ziessel, M. Guardigli, A. Roda, N. Sabbatini, M. Cesario, *J. Am. Chem. Soc.* **2001**, *123*, 2436.

[22] M. Cantuel, G. Bernardinelli, D. Imbert, J.-C. G. Bünzli, G. Hopfgartner, C. Piguet, *J. Chem. Soc. Dalton Trans.* **2002**, 1929.

[23] N. André, R. Scopelliti, G. Hopfgartner, C. Piguet, J.-C. G. Bünzli, *Chem. Commun.* **2002**, 214.

[24] a) A. Beeby, I. M. Clarkson, R. S. Dickins, S. Faulkner, D. Parker, L. Royle, A. S. de Sousa, J. A. G. Williams, M. Woods, *J. Chem. Soc. Perkin Trans. 2* **1999**, 493; b) S. Aime, M. Botta, R. S. Dickins, C. L. Maupin, D. A. Parker, J. P. Riehl, J. A. G. Williams, *J. Chem. Soc. Dalton Trans.* **1998**, 881.

[25] M. Elhabiri, R. Scopelliti, J.-C. G. Bünzli, C. Piguet, *J. Am. Chem. Soc.* **1999**, *121*, 10747.

[26] H. Nozary, C. Piguet, P. Tissot, G. Bernardinelli, J.-C. G. Bünzli, R. Deschenaux, D. Guillon, *J. Am. Chem. Soc.* **1998**, *120*, 12274.

[27] C. Piguet, B. Bocquet, G. Hopfgartner, *Helv. Chim. Acta* **1994**, *77*, 931.

[28] Y. Yamagiwa, Y. Koreishi, S. Kiyozumi, M. Kobayashi, T. Tamikawa, M. Tsukino, H. Goi, M. Yamamoto, M. Munakata, *Bull. Chem. Soc. Jpn* **1996**, *69*, 3317.

[29] a) H. Gampp, M. Maeder, C. J. Meyer, A. D. Zuberbühler, *Talanta* **1986**, *33*, 943; b) H. Gampp, M. Maeder, C. J. Meyer, A. D. Zuberbühler, *Talanta* **1985**, *23*, 1133.

[30] K. Nakamoto, *Infrared and Raman Spectra in Inorganic and Coordination Compounds*, 5th ed., Wiley, New York, **1997**, Part A, p. 199.

[31] J. H. Brewster, *Top. Curr. Chem.* **1974**, *47*, 29.

[32] S. Rigault, C. Piguet, G. Bernardinelli, G. Hopfgartner, *Angew. Chem.* **1998**, *110*, 178; *Angew. Chem. Int. Ed.* **1998**, *37*, 169.

[33] C. Piguet, J.-C. G. Bünzli, G. Bernardinelli, C. G. Bochet, P. Froidevaux, *J. Chem. Soc. Dalton Trans.* **1995**, 83.

[34] M. Pons, O. Millet, *Prog. Nucl. Magn. Reson. Spectrosc.* **2001**, *38*, 267.

[35] Calculated with Equations (2)–(4) and experimental data reported in ref. [17].

[36] a) S. Aime, L. Barbero, M. Botta, G. Ermondi, *J. Chem. Soc. Dalton Trans.* **1992**, 225; b) M. D. Kemple, B. D. Ray, K. B. Lipkowitz, F. G. Prendergast, B. D. N. Rao, *J. Am. Chem. Soc.* **1988**, *110*, 8275; c) M. Allegrozzi, I. Bertini, M. B. L. Janik, Y.-M. Lee, G. Liu, C. Luchinat, *J. Am. Chem. Soc.* **2000**, *122*, 4154.

[37] a) I. Bertini, C. Luchinat, *Coord. Chem. Rev.* **1996**, *150*, 1; b) J. A. Peters, J. Huskens, D. J. Raber, *Prog. Nucl. Magn. Reson. Spectrosc.* **1996**, *28*, 283.

[38] a) C. D. Barry, A. C. T. North, J. A. Glasel, R. J. P. Williams, A. V. Xavier, *Nature* **1971**, *232*, 236; b) J. H. Forsberg, in *Handbook on the Physics and Chemistry of Rare Earths*, *Vol. 23* (Eds.: K. A. Gschneidner, L. Eyring), North-Holland, Amsterdam, **1996**, p. 1; c) J. M. Brink, R. A. Rose, R. C. Holz, *Inorg. Chem.* **1996**, *35*, 2878.

[39] Paramagnetic ^{13}C NMR relaxation measurements failed because of the limited solubility of $[Ln(L^{15})]^{3+}$ in acetonitrile.

[40] W. T. Carnall, P. R. Fields, K. Rajnak, *J. Chem. Phys.* **1968**, *49*, 4443.

[41] a) S. Tobita, M. Arakawa, I. Tanaka, *J. Phys. Chem.* **1984**, *88*, 2697; b) S. Tobita, M. Arakawa, I. Tanaka, *J. Phys. Chem.* **1985**, *89*, 5649.

[42] N. Sabbatini, M. Guardigli, J.-M. Lehn, *Coord. Chem. Rev.* **1993**, *123*, 201.

[43] J. F. Desreux in *Lanthanide Probes in Life, Chemical and Earth Sciences* (Eds.: J.-C. G. Bünzli, G. R. Choppin), Elsevier, Amsterdam, **1989**, Chapter 2, p. 43.

[44] G. Schwarzenbach, *Complexometric Titrations*, Chapman & Hall, London, **1957**, p. 8.

  0947-6539/03/0905-1073 $ 20.00+.50/0

[45] W. C. Wolsey, *J. Chem. Educ.* **1978**, *50*, A335.
[46] A. Altomare, M. C. Burla, M. Camalli, G. Cascarano, C. Giacovazzo, A. Guagliardi, A. G. G. Moliterni, G. Polidori, R. Spagna, *J. Appl. Crystallogr.* **1999**, *32*, 115.
[47] XTAL 3.2 User's Manual (Eds.: S. R. Hall, H. D. Flack, J. M. Stewart), Universities of Western Australia and Maryland, **1989**.
[48] C. K. Johnson, ORTEP II; Report ORNL-5138, Oak Ridge National Laboratory: Oak Ridge, Tennessee, **1976**.
[49] E. R. Malinowski, D. G. Howery, *Factor Analysis in Chemistry*, Wiley, New York, Chichester, **1980**.

Received: September 25, 2002 [F4451]

  0947-6539/03/0905-1074 $ 20.00+.50/0